Corrosion of Stainless Alloys in Potash Brines

A Thesis

Submitted to the College of Graduate Studies and Research

University of Saskatchewan

in Partial Fulfillment of the Requirements

for the Degree of

Master of Science in Chemical Engineering

by

Craig Edward Blackmore

Spring, 1996

In presenting this thesis in partial fulfillment of the requirements for a Postgraduate degree from the University of Saskatchewan, I agree that the libraries of this University may make it freely available for inspection. I further agree that permission for copying of this thesis in any manner, in whole or in part, for scholarly purposes may be granted by the professor or professors who supervised my thesis work or, in their absence, by the Head of the Department or the Dean of the College in which my thesis work was done. It is Understood that any copying or publication or use of this thesis or parts thereof for financial gain shall not be allowed without my written permission. It is also understood that due recognition shall be given to me and to the University of Saskatchewan in any scholarly use that may be made of any material in my thesis.

Requests for permission to copy or to make other use of material in this thesis in whole or part should be addressed to:

The Head of the Department of Chemical Engineering
University of Saskatchewan
Saskatoon, Saskatchewan
Canada
S7N 5C9

ACKNOWLEDGMENTS

I would like to thank my supervisor, Dr. Jack Postlethwaite, for his guidance and support throughout my work. I would also like to thank the other members of my advisory committee, Dr. S. Yannacopoulos and Dr. D.Y. Peng.

Financial support was provided by the Saskatchewan Potash Producers Association. The experimental results of this work are included as part of S.P.P.A. project U266. Laboratory facilities were provided by the Department of Chemical Engineering, University of Saskatchewan. Pilot plant and potash mill facilities were provided by the Potash Corporation of Saskatchewan.

to my Family

ABSTRACT

The temperatures and concentrated chloride environments involved in potash milling provide conditions for high susceptibility to localized corrosion. This must be countered with careful material selection that provides adequate protection at affordable cost. Indexes have been formulated to take into account the effect of the elemental composition of a passive alloy on the resistance of the alloy to localized corrosion. A very comprehensive index, the Localized Corrosion Resistance Index (LCRI), is studied by this thesis and is evaluated for its accuracy in ranking stainless alloys.

The LCRI, Cr%+3.3(Mo%)-0.33(Ni%)+16(N%), takes advantage of the readily available weight percentages of chromium, molybdenum, nickel, and nitrogen. This thesis examined the theories behind pitting and crevice corrosion and the effect these elements have on the passive layers protecting the surface of a stainless alloy. Electrochemical experiments were performed on selected alloys in laboratory conditions, a pilot plant flow loop, and in potash mill conditions.

The data obtained for this thesis supported the use of the LCRI as a ranking index for austenitic and duplex stainless steels. Ferritic and cast austenitic steels had less resistance to localized corrosion than the LCRI indicated. Totally different indexes or radical correction factors would be required to allow comparison of all types of alloys. A separate and extensive study could eventually achieve this.

Temperature effects were examined to determine if the ability to accurately rank alloys with the LCRI could be compromised. The experiments tracked the pitting resistance of the alloys over a temperature range of 20-100°C, covering conditions found in potash mills. The results found the LCRI reliable over the whole range of temperatures.

Chromium, molybdenum, nickel, and nitrogen factors in the LCRI were studied, each in turn, to evaluate their worth in predicting the localized corrosion behavior of passive alloys. The data supported the theories regarding the effect of each element on the passive layer protecting the surface of the alloys. A new index was formulated to better fit the experimental data. The formula Cr%+4.1(Mo%)-0.14(Ni%)+6(N%) indicates molybdenum had a more pronounced effect on corrosion resistance while nitrogen's beneficial effect and nickel's detrimental effect were less pronounced. This formula, denoted LCRI11, offers better accuracy than the more conventional LCRI.

Table of Contents

List of Tables

List of Figures

List of Abbreviations

LCRI --- Localized Corrosion Resistance Index

= Cr%+3.3(Mo%)-0.33(Ni%)+16(N%)

LCRI2 --- Localized Corrosion Resistance Index Modification

= Cr%+3.3(Mo%)-0.33(Ni%)+30(N%)

LCRI3 --- Localized Corrosion Resistance Index Modification

= Cr%+3.3(Mo%)-0.33(Ni%)

LCRI4 --- Localized Corrosion Resistance Index Modification

= Cr%+3.3(Mo%)+16(N%)

LCRI5 --- Localized Corrosion Resistance Index Modification

= Cr%+3.3(Mo%)

LCRI6 --- Localized Corrosion Resistance Index Modification

= Cr%

LCRI7 --- Localized Corrosion Resistance Index Modification

= Cr%+4.1(Mo%)

LCRI8 --- Localized Corrosion Resistance Index Modification

= Cr%+4.1(Mo%)+6(N%)

LCRI9 --- Localized Corrosion Resistance Index Modification

= Cr%+4.1(Mo%)+6(N%)-0.1(Ni%)

LCRI10 --- Localized Corrosion Resistance Index Modification

= Cr%+4.1(Mo%)-0.14(Ni%)

LCRI11 --- Localized Corrosion Resistance Index Modification

= Cr%+4.1(Mo%)-0.14(Ni%)+6(N%)

LCRI12 --- Localized Corrosion Resistance Index Modification

= Cr%+3.3(Mo%)+2(N%)

E_{np} --- Breakdown potential, also described as the pitting potential

E_{pp} --- Repassivation potential

CPT --- Critical Pitting Temperature

CCT --- Critical Crevice Temperature

Sh_{avg} --- Sherwood Number (based on an average mass transfer coefficient

Sc --- Schmidt Number

Re --- Reynolds Number

d_e --- equivalent diameter

L --- mass transfer length

a, b, c, and d --- constants determined by correlations

I_{corr} --- corrosion current

R_p --- polarization resistance

b_a --- anodic Beta coefficient

b_c --- cathodic Beta coeffient

Chapter 1. Introduction

This study utilized electrochemical testing methods to determine the resistance of various alloys to localized corrosion in potash brine. Localized corrosion includes pitting and crevice corrosion. This type of corrosion leads to equipment failure and replacement costs, through material loss and initiation of stress corrosion cracking.

Metal alloys can be ranked according to their resistance to localized corrosion using an index based on the composition of the alloy. Alloys with a wide range of compositions were chosen to be tested for resistance to localized corrosion to evaluate ranking indexes for the potash industry. The primary index investigated was the Localized Corrosion Resistance Index, LCRI, Cr%+3.3(Mo%)-0.33(Ni%)+16(N%), proposed by Nadezhdin and Wensley [1]. They had developed the LCRI from Lorenz and Medawar's index, Cr%+3.3(Mo%)+16(N%). The major focus of this work required controlled laboratory testing. Some experiments in a pilot plant flow loop and in a potash mill supplemented the data.

1.1. Objectives

The experimental work, as detailed in Chapter 3, was categorized into the following sections:

1.1.1. Laboratory Study

A one litre bench top glass cell apparatus utilizing a rotating cylindrical electrode provided an easily controlled environment for testing alloys. The effect of temperature on the pitting potentials was a key interest in this study. Temperature has not been factored into the corrosion resistance index formulas. The intent of this project is to determine if temperature has a significant impact on the validity of using composition indexes in rating alloys for use in corrosive environments. The laboratory experiments were performed over a range of temperatures from room temperature to 90-100°C, covering the conditions expected in a potash mill.

1.1.2. Pilot Plant Study

A 101.6 mm (4") schedule 40 test spool with electrodes set flush with the pipe wall was used in a flow loop at the PCS Pilot Plant. Experiments on various alloys were performed to determine resistance to localized corrosion and to determine uniform corrosion rates. Passive and non-passive alloys were tested under these conditions.

1.1.3. Potash Mill Study

This project involved some work at the Cory Potash Mill to prove that the portable potentiostat could be used in a full scale plant. The Gamry CMS100™ corrosion measurement system performed to expectations under potash mill conditions.

Chapter 2. Literature Survey

2.1. Passivation and Pitting Corrosion of Stainless Alloys

There are several theories regarding the pitting and passivation of metals. Conclusive information from experiments has yet to be found that proves any existing theory or establishes a new theory that explains every aspect of passivation or pitting. The theories can be divided into those that state passivation of metals is the result of a competitive adsorption process and those that state a three dimensional passive film is necessary to represent the true process.

The adsorption model would only require a monomolecular film, whereas the three-dimensional film would have a thickness of 10 to $100A$. Passive films have been measured and found to be about $50A$. This does not prove the thick film theories to be correct. The actual passivation may depend entirely on an underlying monomolecular layer, with the thick layer being a by-product of the process [2].

Adsorption theories describe the surface of the metal as being covered in a layer of water molecules, oxygen molecules, ions and organic molecules (impurities). The water molecules are weakly adsorbed to the surface, but the ions and impurities can be strongly attached. These species block sites where the electron absorbing particles can reach the surface and receive an electron. This causes the initial free

energy of the electron transfer reaction to drop, and the activation energy will be larger for reactions farther away from the surface.

Pitting is a process that is initiated when chloride ions displace the other particles. The pitting potential is the potential at which sites previously taken by passivating particles are replaced by aggressive anions that allow metal dissolution. Experiments have indicated that at potentials below the critical pitting potential, chloride ions may be assisting the passivation by adsorbing on the surface and blocking sites for metal dissolution. As the potential exceeds the pitting potential, E_{np}, the chloride becomes activated and metal is allowed to dissolve. This accounts for the increase in the number of pits per unit area as the chloride ion concentration increases. More chloride occupying more sites on the metal surface allows for more initiation sites. The more chloride ions adsorbed to the surface, the worse the pitting will be when the potential rises above E_{np} [3].

Three dimensional passive films add penetration and migration processes to the theory. The chloride ions have to move through the passive film to reach the surface. This is explained by permeation, diffusion by dislocations, chloride-oxygen exchange, lattice migration, and electrostatic fields, depending on the theory one chooses to apply. All have exceptions and limitations [4].

If the assumption is made that the protective film is thick enough to be modeled by a three dimensional film, the following process can be used to describe pitting:

During pit initiation, the anodic area creates a depression in the surface as the metal dissolves into the electrolyte. The dissolving metal ions can react to form a passive oxide/hydroxide film, or a non-protective gelatinous hydroxide precipitate. The reactions creating the passive product and the gelatinous material consume hydroxide ions. This promotes the hydrolysis of water, producing hydrogen ions and reducing the pH. The hydrogen ions partake in the cathodic reactions with electrons and oxygen to produce water. The low pH and presence of chlorides promote metal dissolution that causes further reduction in the pH. This self-fueling process is described as being autocatalytic.

The pit passes through three phases in its growth. After initiation, the reactions producing non-protective gelatinous films dominate. The dissolving metal is used to form the gel-like film rather than replenish the passive film. The gel-like film readily conducts ions, but it prevents the metal from dissolving quickly. The dissolution becomes the rate-determining process. As the gelatinous film replaces the passive film, the dissolution rate increases, and the pit deepens. At the start of the second stage, the passive film is completely gone, and the vicinity of the pit is saturated with cations and anions. The ion migration is now slower, and the dissolution rate is faster. The slow conduction of the ions hampers the process and becomes the rate-determining step for the process. This is the point when the pit becomes autocatalytic. The pit continues to grow. The third phase is reached when the repassivation reaction rate surpasses the gel-like film production. The pit reaches its maximum depth. The passive layer coats the pit surface and replaces the gel-like

layer. The metal dissolution rate slows down and again becomes the rate-determining process [5].

A model describing the effect of chloride ions on the mechanisms of pitting corrosion has been developed. This model is based on the theory that chloride reacts with the dissolved metal ions to form an intermediate compound. This compound quickly reacts to form a gelatinous hydroxide film and releases the chloride ion back into solution. The unprotective gelatinous film competes with the passive film for space on the metal surface. The higher the concentration of chloride ions in the vicinity of the pit, the more favorable the production of the gelatinous product. Eventually, the passive film can not be produced fast enough and the gel-like film covers the surface of the pit. This allows the metal to dissolve faster from the unprotected surface [6].

It is known that water molecules are bound into the structure of the passive film, as are hydronium ions. The proposed models for the protective film structure are shown below, including the way in which water grants the film the ability to repair itself. Chloride ions are seen to assist breakdown when they replace enough water and hydronium [4].

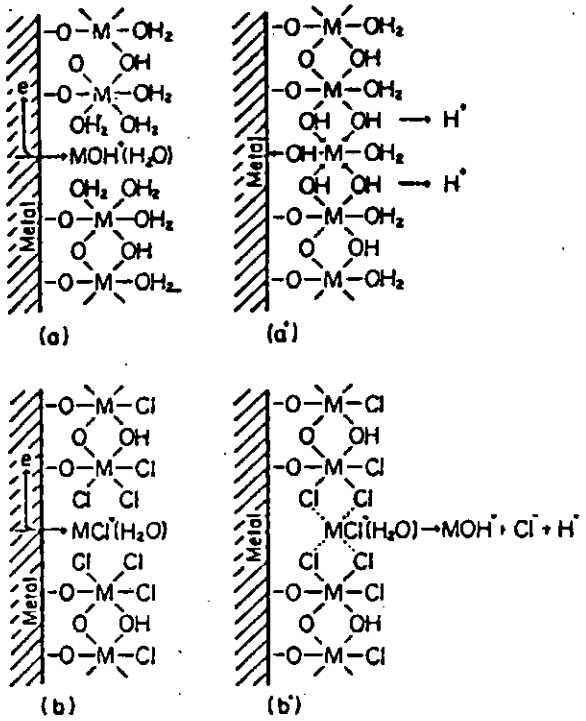

Figure 2.1 Models of the Passive Film
(a) Dissolved metal ions, $MOH^{+}(H_2O)$, are captured to form the film (a')
(b) Chloride ions substituted for H_2O molecules inhibit OH bonding to metal (b'), resulting in breakdown of the passive film
[Source: Z. Szklarska-Smialowska. Pitting Corrosion of Metals. 1st ed. National Association of Corrosion Engineers, p. 382 ,1986]

Theories relating to chemical dissolution deal with the formation of metal-anion complexes. For austenitic stainless steels, a relationship was found between the induction time and the chloride concentration in the electrolyte that brought forth the conclusion that three or four chloride ions must surround a metal cation in the lattice with one of them also replacing an anion (like the O^{-2} in Figure 2.1) between the cation and the surface. This allows the cation to dissolve more easily as it has fewer

surrounding oxide ions from which to separate. Separation from halides is easily achieved. The newly created gap in the passive layer is filled with a new cation from the surface. The chloride ions are still in place around the gap, and all replacement cations can be dissolved as readily as the first. The halide surrounded site is a location of high energy. This site will not be created easily, but once in place, many metal ions are lost through it. A new pit has been initiated [7].

By analyzing light reflected off an electrode, and examining data on the current and potential, one gains more insight as to how passivation works. A thin film of $Ni(OH)_2$ can be seen to form on nickel in an acidic solution. This film is created at potentials below the passivation potential, and it offers no protection. Above the passivation potential, the film becomes a stable, protective film, and the electrode is passivated. The light reflection experiments show another change in the film as it exceeds the passivation potential. The "prepassive" film does not absorb light, but the passive film does. This substantiates that there is a difference in the physical properties of the films. This can be explained if the prepassive film had no free electrons to absorb the light, and the passive film did. The prepassive film would be an electronic insulator, and the passive film an electronic conductor. The insulator film has a large potential drop that drives the dissolution of the metal from the surface to the electrolyte. Once the passivation potential is exceeded, the film increases in conductivity and the potential drop across the film decreases. With no driving force, the dissolution rate decreases and the film becomes passive. The electronic conductivity of the film is crucial for effective passivation [8].

When pitting initiates, the passive film is broken down on many small sites. High anodic currents flow to these sites to cause pitting. Electromigration also plays an important role. More chloride ions are drawn to the pit and cations are driven out of the pit. The more metal dissolved, the more this migration process is promoted. Hydrodynamics affect pitting by washing out the pits and allowing for repassivation [6].

Theory dictates that a large IR drop for the system is necessary for pitting. In reality, the pit is short-circuited with anodic and cathodic potentials approach one another until the difference between them is only the IR drop of the electrolyte, which is usually small. Vetter and Strehblow [9], and Ives and Strehblow [10] suggest that an anodic reaction taking place in the passive region in the presence of chloride ions can allow for pits with small IR drops.

Careful assessment of these theories leads one to the support of the three-dimensional film model. It describes mechanisms that explain the formation and breakdown of the passive layer satisfactorily. The absorption theories provide an alternative viewpoint to passivation of alloys. Until research into passivation mechanisms reveals clearer answers and one theory is substantiated, the three-dimensional model should be considered first when approaching corrosion problems.

2.1.1. Effect of Alloy Composition

The major focus of this thesis is the evaluation of stainless alloys using indexes based upon the elemental compositions of the alloys. Each element in the metal lattice must be quantified as to its relative positive or negative effect on the formation and stability of the passive layer. The major contributors to most indexes are chromium, molybdenum, nitrogen, and nickel. A review of the less common elements as well as the effect of duplex structure is detailed below.

2.1.1.1. Chromium

The benefits of chromium in forming stable passive films are well known. It is a metal suited to form a stable matrix for the passive layer of the type seen in Figure 2.1. At least 12% Cr by weight is needed to make a stainless steel.[1] Increasing the chromium content increases the corrosion resistance of the alloy.

2.1.1.2. Molybdenum

Molybdenum is also important as a protective component in stainless steels. Dramatic improvement is seen with the addition of the first 2% of Mo. Further improvement is made up to about 6% Mo. Adding more than this reportedly hinders corrosion resistance. Figure 2.2 indicates the Cr-Mo relationship.

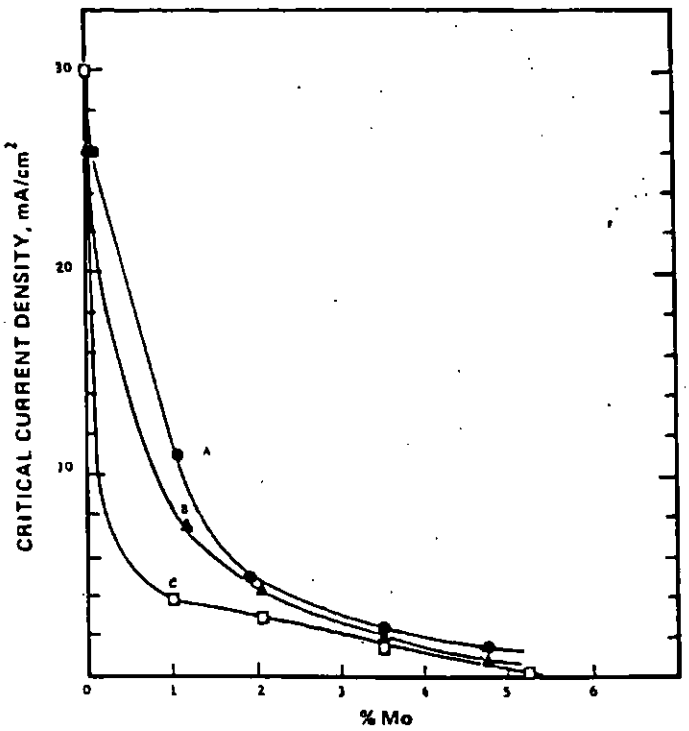

Figure 2.2 Critical Current Density vs. Molybdenum Content
for High Purity Stainless Steel in 1N H_2SO_4 at 29.8°C
A = 13Cr, B = 18CR, C = 25Cr
[Source: Steigerwald, Bond, Dundas, and Lizlovs. Corrosion, Vol. 33, p. 279 (1977)]

Adjusting the emphasis of molybdenum in corrosion resistance indexes for the 0 to 2%, 2 to 6%, and 6%+ ranges could improve the accuracy of the indexes. A universal formula applicable to all ranges of molybdenum is required for a corrosion resistance index created for widespread usage, making such adjustments impractical. If the variety of alloys that an index was to be applied to was restricted, such adjustments could be justified.

Molybdenum may affect passivation and corrosion resistance by two mechanisms. The molybdenum in the alloy may cause the passive film to become enriched with molybdenum ions that can change the characteristics of the film through their interactions with the ions attempting to pass through the film. Enrichment of Mo in the alloy on the surface just below the passive film would affect the adsorption properties of the alloy. Experiments outlined by Urgen and Cakir[11] were designed to test these possibilities. Adding molybdenum ions to the electrolyte solution of 304 stainless steel would give it the same pitting behavior as 316 stainless steel without additional molybdenum ions since the basic difference in the two alloys is their Mo content. Their experimental results showed that the behavior of the 316 could be mimicked by the 304 with an appropriate electrolyte. Another experiment testing the adsorption theory was based on the idea that sulfate ions would have similar inhibitive properties as molybdate ions since the sulfate is known to affect adsorption. The sulfate ions were less effective with increasing temperature, but the molybdate ions improved. Urgen and Cakir[11] reasoned that the protective properties of Mo would then be at least partially based on the effects of the ions on the film characteristics and not based on surface adsorption.

Molybdenum ions can affect the properties of the film in different ways. They act to raise the pH by the following reactions:

$$7MoO_4^{2-} + 8H^+ \rightarrow 4H_2O + Mo_7O_{24}^{6-} \qquad (2.1)$$

$$Mo_7O_{24}^{6-} + 3H^+ + HMoO_4^- \rightarrow Mo_8O_{26}^{4-} + 2H_2O \qquad (2.2)$$

The molybdenum ions also react to form molybdic acid which precipitates out of solution and blocks active sites on the surface. The formation of molybdic acid is faster at higher temperatures. This accounts for their experimental results. The dissolution of a film containing molybdates and molybdic acid will decrease because of their low ion conductivity [11].

2.1.1.3. Nitrogen

Nitrogen is another component that provides additional protection. Increasing chromium does not affect the size of repassivated pits. Increasing nitrogen content decreases the size of the repassivated pits. One concludes that nitrogen has an effect on metastable pits that chromium does not have. Nitrogen also enhances resistance to pit initiation. The production of NH_4^+ inside pits has been observed and documented. This production was seen to decrease with increasing applied potentials. An apparent Tafel slope for the reaction

$$N + 4H^+ + 3e^- \rightarrow NH_4^+ \qquad (2.3)$$

could be found. This reaction is slow, and the surface becomes enriched with nitrogen. The nitrogen blocks anodic dissolution sites and high current densities are prevented. Repassivation would also be assisted by nitrogen enrichment because when the current finally increases, it increases rapidly to extremely high values, and the dissolution of iron is the preferred reaction. Greater chromium enrichment at the surface of the pit occurs during the onset of localized corrosion. This high chromium concentration near the surface promotes repassivation. Alloys lower in nitrogen do

not get this initial drop in iron concentration that increases the concentration of the other species at the surface [12].

2.1.1.4. Nickel

Nickel is added to steel primarily for its strength increasing properties and its ability to promote the formation of an austenitic phase. The corrosion resistant properties of nickel lie in the prevention of stress corrosion cracking and use in high temperature acids. Localized corrosion is promoted by nickel in most instances. The inclusion of nickel in corrosion resistance indexes has had mixed interpretations. It has been considered a positive influence for its resistance to general corrosion and a negative influence for its susceptibility to pitting and crevice corrosion in stainless steels. The localized corrosion indexes are only designed to apply to the resistance of the alloy to pitting and crevice corrosion, and should incorporate the negative influence. Care should be taken not to use localized corrosion resistance indexes when conditions favor other forms of corrosion over pitting and crevice corrosion.

2.2.1.5. Residual Elements

The resistance of stainless steel alloys to localized corrosion can be enhanced or compromised by the presence of residual elements from the forming process and those purposefully added to improve the mechanical properties of the alloys. Moskowitz et al. [13] proposed that the phase of the residual element is the most important factor that determines how the element will affect pitting resistance. They

reviewed existing data in literature and performed their own experiments, which included electrochemical tests.

Elements that form a non-metallic second phase appear to reduce the pitting resistance of the alloy. Moskowitz et al. [13] reported cerium, columbium, selenium, sulfur, tellurium, and titanium as exhibiting such behavior. The imperfection in the metal lattice resulting from a second phase of any of these elements could result in the creation of a very small galvanic cell to initiate a pit. An element that forms a metallic second phase would not pose as serious of a problem. Lead and silver were the only elements investigated by Moskowitz et al. [13] that fell into the metallic second phase category, and silver proved to enhance pitting resistance.

The beneficial elements included in their study were molybdenum, nitrogen, silicon, rhenium, and vanadium. The increase in resistance was attributed to the fact that these elements are all in solid solution. This would allow these elements to enter the passive film and contribute to its stability. Another explanation for elements in solid solution strengthening pitting resistance comes from Tomashov et al. [14]. Their explanation regards the grain boundaries. The structure and composition differences between the grain boundaries and the lattice within the grain can facilitate the formation of a tiny electrochemical cell. The grain behaves cathodically and the boundary behaves anodically. The presence of residual elements in solid solution rather than a second phase would add to the homogeneity of the grain and decrease the likelihood of pits initiating from one of these tiny grain-cells. Cobalt, lead, phosphorous, tantalum, tin, tungsten, and zirconium all exist in the solid solution, but

had essentially no effect according to the Moskowitz et al. [13] study. No explanation could be found for the question of why some solid solution elements increased pitting resistance and others did not. They may all affect the resistance properties of the alloy by the same mechanism, but to varying degrees; some of which are negligible.

Three elements involved in the Moskowitz et al. [13] study had more than one effect depending on the conditions. Carbon and boron could be in solution or could form harmful non-metallic precipitates. When in solution, carbon had no effect on pitting while boron was beneficial. Copper appeared to behave differently depending upon the presence of molybdenum in the alloy. Copper did not affect pitting unless molybdenum was part of the alloy. Increasing copper content undermined the localized corrosion resistance of the alloy.

Tomashov et al. [14] performed experiments on residual elements in 18Cr-14Ni alloy by varying the concentration of residual elements added to a stock of 18Cr-14Ni alloy. Their tests were in 0.1N NaCl at 25°C. Rhenium, vanadium, molybdenum, and silicon all enhanced pitting resistance in the order of rhenium the most and silicon the least protective. Very small amounts of titanium helped, but the advantage decreased after 0.3%Ti. Wolfram was detrimental in amounts less than 1%, but helpful at higher weight percentages. Niobium, cerium, and tantalum all had negative effects on the alloy.

Most of the elements investigated by Tomashov et al. [14] and some investigated by Moskowitz et al. [13] were not common among the alloys selected for

this project. The studies did provide validation for the theories on residual element phases and grain boundaries affecting localized corrosion resistance. These are the lesser factors that can influence the development of a resistance index. The effect of residual elements on pitting can be overshadowed by external factors and case specific conditions. However, knowing the pronounced effect molybdenum has on the performance of chromium, residual elements should be studied to determine the role they play in the passivation of alloys.

2.1.1.6. Compositions Within Duplex Stainless Steels

There is some difficulty in assessing the corrosion resistance of duplex stainless steels by the composition of the elements in the alloy. The formation of two phases within the alloy is affected by the elements that create them. In an austenitic-ferritic duplex alloy, the elements that promote the formation of the austenitic phase will exist in a higher concentration in that phase than in the ferritic phase, and vice-versa. Bernhardsson [15] noted the higher concentrations of nickel, nitrogen and copper, and the lower concentrations of chromium, molybdenum and silicon in the austenitic phase compared to the ferritic phase of 2205 Duplex. Some duplexes have very similar compositions in both phases, such as 2507 Duplex. The problem of which phase corrodes more easily and why complicates the matter. Bernhardsson [16] suggested that the nitrogen factor in duplex steels was more pronounced, and index equations for duplexes should use 30 as a multiple of the percent weight nitrogen while other stainless steels should use 16. This was to account for the higher nitrogen content in the austenitic phase, which he reported as the more susceptible

phase due to the loss of chromium to the ferrite. The experiments in this study showed that ferritic alloys are less resistant to localized corrosion than austenites with the same chromium content. This indicates that the ferrite phase in duplex alloys could still be the more susceptible phase despite the higher chromium content, undermining Bernhardsson's reasoning behind the use of separate indexes for duplex and austenitic alloys.

2.1.2. Temperature Effects

Temperature has considerable effects on the kinetics of pitting. At higher temperatures, a broader distribution of cathodic current occurs over the surface of the alloy and more pits initiate. Researchers have observed that pits formed under these conditions are not as large as those formed under lower temperatures. The pits may be smaller due to the increase in the ohmic polarization of the electrolyte and the increase in corrosion products with temperature. Chloride chemisorption is believed to be stronger at higher temperatures, enhancing breakdown of the passive layer. These are two possible processes that are weakly temperature dependent and could influence the pit growth [17].

The concepts of Critical Pitting Temperature and Critical Crevice Temperature, CPT and CCT, were developed in the 1970's by Brigham and Tozer [18]. They represent critical points where the temperature allowing passive behavior of a metal is exceeded and pitting or crevice corrosion is expected. However, it is still not confirmed that the points are absolutely critical and not transition points for ranges of temperature that promote pitting or support stable passive films. Figure 2.3

shows critical crevice temperatures for 316 and 304. The experimental conditions for this study had a chloride content higher than the scale of Figure 2.3, and temperatures that would be well within the crevice corrosion region.

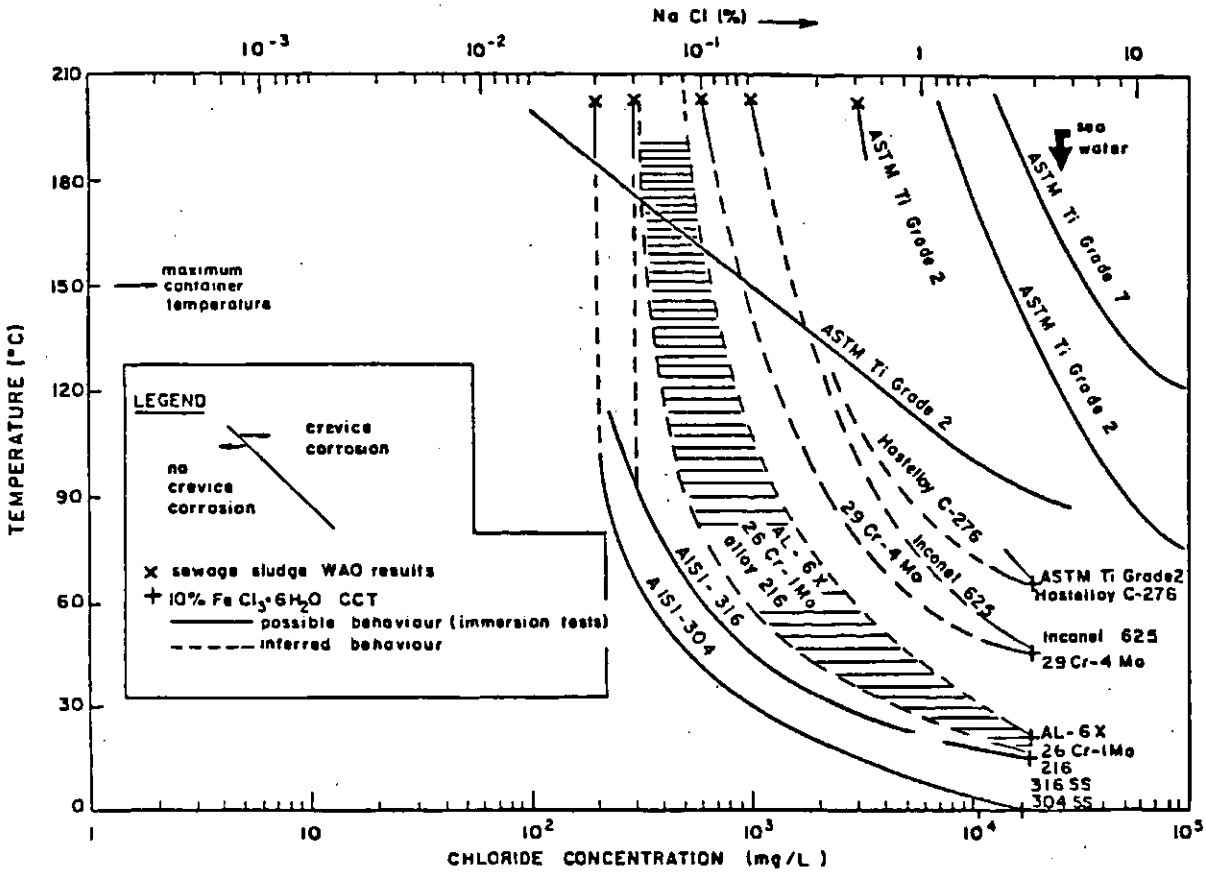

Figure 2.3 Critical Crevice Temperatures for Various Alloys in Chloride Solution [Source: J. Postlethwaite.Technical Report AECL-9952 "Localized Corrosion of Alloys C-276 and 625 in Aerated Sodium Chloride Solutions at 25 to 200°C", Whiteshell Laboratories, Pinawa MB, p.24 (1991)]

The ranking indexes such as the Localized Corrosion Resistance Index do not take temperature into consideration. The possibility of a highly rated alloy suffering a reduction in resistance at higher temperatures making other alloys more favorable for use at high temperatures has to be considered. The experiments undertaken for this thesis were performed over a range of temperatures to expose possible problems with the indexes.

2.2. *Surface-Solution Mass Transfer*

A rotating cylindrical electrode was used for the working electrode in the laboratory experiments. By using dimensionless numbers in an experimental correlation, the proper rotating velocity can be selected to simulate the solution to surface mass transfer rates for pipes of different diameters. The equations have the form

$$Sh_{avg} = a(Sc)^b(Re)^c (d_e/L)^d \tag{2.4}$$

where a, b, c, and d are constants determined by correlations and verified in experiments by G.R. Youngquist [19].

Chapter 3. Experimental

3.1. Gamry CMS 100 Corrosion Measurement System

The Gamry CMS100 Corrosion Measurement System™ was used for all experiments. The Gamry™ has its own potentiostat/galvanostat housed in a portable PC. The software controlling the test routines is operated within Microsoft Windows®. Data from a test routine is stored in Microsoft Excel® allowing easy manipulation of the data. Some analysis and calculations can be performed by the software included with the Gamry™. For example, Tafel slopes can be fit to the potential versus log(i) curves, and polarization resistance and corrosion rates can be calculated. There are twelve standard experimental techniques available with the Gamry™. These could be modified or new routines created by using the specialized script language Explain™ which was developed for controlling electrochemical test equipment. The present project required data on localized corrosion resistance and uniform corrosion rates. The standard test routines, cyclic polarization and polarization resistance (linear polarization), provided this information.

3.2. Laboratory Bench Top Glass Cell

3.2.1. Laboratory Apparatus

The laboratory apparatus included a conventional three electrode electrochemical test cell, as seen in Figure 3.1. The two side views show the six ports as arrayed in the top view below:

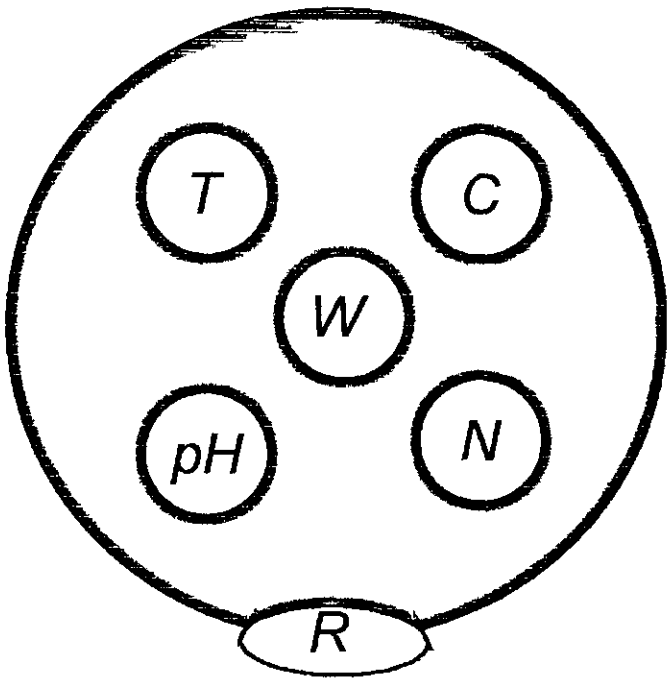

3.1a. One Litre Bench Top Glass Cell, Top View

Where T is the thermometer port
C is the counter electrode port
W is the working electrode port
pH is the pH meter port
N is the port for the nitrogen feed and gas outlet through condenser
R is the port for the salt bridge to the reference electrode

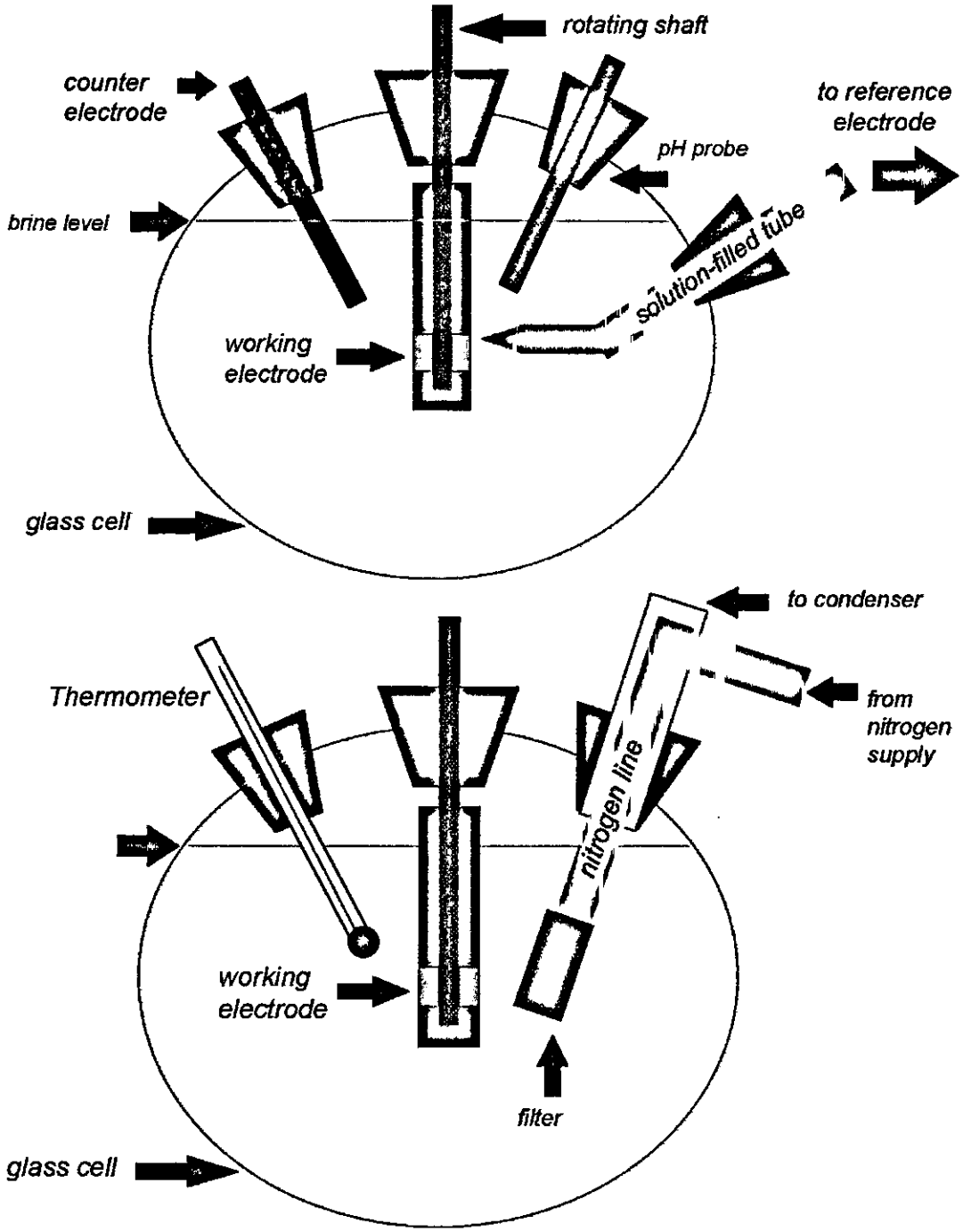

Figure 3.1b and 3.1c One Litre Bench Top Glass Cell, Side Views

A Pine Instrument Company[1] AFMSRX rotating cylindrical electrode apparatus was used to house the working electrode. By using dimensionless numbers in an experimental correlation, the proper rotating velocity was selected to simulate the solution to surface mass transfer rates for brine flowing at a specified rate in a pipe of specified diameter. The potentiostat required electrical connection to the working electrode. This was done through metal brushes in contact with the metal rotating shaft holding the cylindrical working electrode. The electrodes had a $3cm^2$ surface area polished to 600grit.

The reference electrode was a Fisher[2] silver / silver chloride electrode. The quality of the silver / silver chloride reference electrodes was checked periodically by comparing the potential difference to a Fisher[2] calomel electrode. The use of a salt bridge to distance the reference electrode allowed the reference electrode to remain at room temperature. All laboratory experiments are then referenced against a silver / silver chloride electrode with an internal electrolyte of 4M NaCl and saturated AgCl at 20°C. The counter electrode was a graphite bar.

3.2.2. Laboratory Test Conditions

3.2.2.1. Materials

The materials selected for the laboratory testing are shown in Table 3.1 with their component elements given in weight percentages. The selection was based on the LCRI values of the materials. A range of LCRI values was required to establish a

[1] Pine Instrument Company, Grove City, PA.16127
[2] Fisher Scientific Canada, 112ch. Colonnade Rd., Nepean, ON U2E 7L6

significant data base for analysis. The materials 304LN and 316LN were included to provide a better analysis of the effect of nitrogen composition as they have nitrogen purposely added, but are otherwise similar to 304L and 316L. Duplex alloys were of interest to the potash industry, as was 904L, 254SMO and the cast alloys.

Table 3.1 Element Compositions of Alloys used in Laboratory Study
(more data on compositions and heat treatment available in Appendix A)

	Metal Compositions % weight				
Alloy	Cr	Ni	Mo	N	LCRI
Austenitic					
347 ss	17.1	10.0	0.2	---	14.6
304L	18.2	8.8	0.2	0.063	17.1
304LN	19.8	8.8	0.4	0.124	20.2
316L	17.5	11.7	2.3	0.085	22.5
316LN	16.5	10.2	2.1	0.119	21.9
904L	20.3	24.0	4.3	---	26.6
254SMO	20.1	18.0	6.2	0.200	37.7
Ferritic					
430 ss	16.6	0.3	0.0	0.037	17.2
446 ss	26.0	0.0	0.0	0.180	28.9
Cast Alloys					
CD4-MCu	25.5	5.0	1.9	---	30.0
CN7M	20.0	28.8	2.2	---	17.7
Duplex					
2304	22.5	4.5	0.4	0.120	24.1
2205	22.2	5.6	3.0	0.150	32.7
Precipitation Hardened					
17-4 PH	15.4	4.3	0.4	---	15.4

3.2.2.2 Solutions

The laboratory testing used a standard 'simulated potash brine' made from reagent grade chemicals prepared as an approximation of typical brines found in mills around Saskatchewan. The standard potash brine was prepared by combining the following mixture to the required weight:

Table 3.2 Standard Potash Brine

Compound	Weight %
Na_2SO_4	0.56
KCl	16.58
NaCl	26.54
$MgCl_2$-$6H_2O$	3.34
$CaCl_2$-$2H_2O$	0.59
H_2O	52.38

The tests were performed over a range of temperatures between 20°C to 100°C. The experiments were supplemented by data gathered using circuit brine collected from three Saskatchewan potash mills for comparison with the 'simulated' brine. The brines used came from Cory, Vanscoy, and Viscount Mills courtesy Potash Corporation of Saskatchewan, Cominco, and Central Canada Potash respectively.

3.2.3. Experimental Procedure

The experimental regimen was as follows: The alloy to be tested was wet polished with 600 grit abrasive paper and checked under magnification for polish marks to ensure quality polishing was performed. The electrode was immersed in the brine and the deaeration initiated. Nitrogen gas (99.999%) was bubbled into the cell through the gas inlet to remove the oxygen from the system and create the deaerated environment. One hour of deaeration was allowed before electrochemical testing began. During this hour, the rotator spun the electrode at the same speed setting at which the test would be conducted.

The tests began at room temperature. After the first scan, the heater was turned on and the temperature increased. When the desired temperature was reached, manual manipulation of the heater's auto transformer provided a stable temperature. The data was used to develop pitting potential versus temperature trends.

The temperature was increased between experiments because decreasing the temperature allowed crystal formation on the pH probe and thermometer, probably interfering with their efficiency.

The electrochemical test routine performed in the laboratory was the Cyclic Polarization test. The parameters of the test were as follows: The initial voltage was set at -0.6V, the apex of the voltage sweep was set at 1.5V, and the final voltage of the return sweep was -0.5V. After conducting the first test, these voltage settings could be fine tuned to the specific alloy being tested to reduce extraneous data collection and save time. A scan rate of 0.5mV/s was used. A faster scan rate than outlined in the ASTM standards was chosen to allow more tests to be performed on an electrode in one day. A current density ceiling of $0.1 mA/cm^2$ was used to prevent the current density from increasing to the point where the corrosion reaction would seriously damage the electrode surface. If the current density exceeded the ceiling for a certain time period, the Gamry CMS100™ would automatically reverse the potential sweep and the current density would eventually drop as the pits repassivated.

Information in addition to the electrochemical data was recorded at the initiation and completion of the test run. This included the temperature and pH of the brine, as indicated by the thermometer and the pH probe. No buffer solution was

added to the brine, and the natural pH of the brine was slightly higher than the pH values of neutral water taken from Potter [20]. The experiments had an impact on the pH of the brine, and, occasionally, corrective action was taken by adding a small quantity of sodium hydroxide. If the sodium hydroxide increased the pH higher than what was acceptable, hydrogen chloride was used to reduce the pH. An adjustment of this kind can be seen in Figure 3.2 for the experiments for the 17-4 Precipitation Hardened steel. The alloy suffers breakdown and pitting corrosion readily, as seen by the pitting potentials in Figures 4.1a and 4.1b. The current densities for the cyclic polarization scans were quite high, indicating more metal dissolution, which was confirmed by visual inspection of the electrode after the test. The higher concentration of metal ion would bond with more hydroxide to promote the hydrolysis of water, and the increase in hydrogen ions would lower the pH. The largest pH drop occured during the 40°C test, from 6.76 to 6.11 . Addition of sodium hydroxide brought the pH up to 7.11 for the 50°C test, but after the 50°C experiment, it returned to the previous trend.

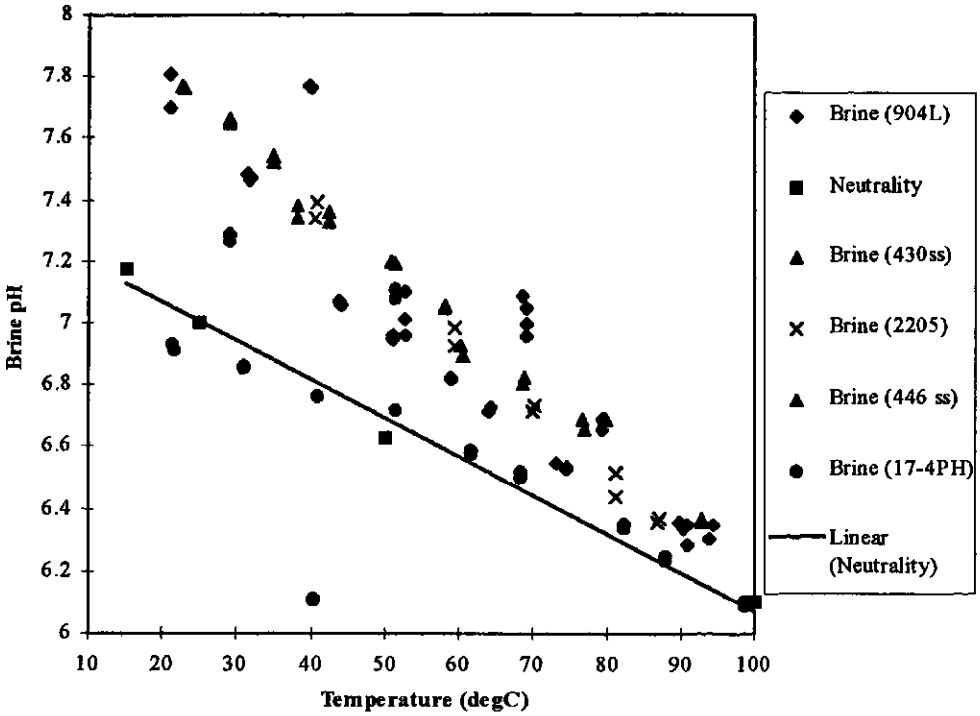

Figure 3.2 Brine pH vs Temperature for Five Experiments and Neutral Water

3.3. Pilot Plant and Potash Mill Flow Cells

3.3.1. Test Spool

The test spool and the electrode decks for the pilot plant and potash mill studies are shown in Figures 3.3 and 3.4. Two spools were built, Spool #1 has only one electrode deck, and Spool #2 has three electrode decks. The electrodes are cylindrical and set into the deck aligned along the radius of the pipe. The 'inside' circular surface is exposed to the brine and is flush with the pipe wall. This provides a flat test surface of known area ($0.71cm^2$). The curvature of the 101.6mm (4") schedule 40 pipe wall is approximated by a flat surface for simplicity of fabricating the test samples. Any flow disturbance caused by the change in surface is considered to be negligible. The 'back' surface of the electrode is threaded to a lead that makes the contact to the potentiostat that is necessary to complete the circuit. The treaded leads serve the additional purpose of bolting the electrode tightly in place. Teflon sleeves surround the electrodes and the leads to isolate them from the metal deck. As each deck holds three electrodes, the center electrode was always used as the reference electrode. The other two electrodes were used as the working and counter electrodes, switching between the two, doubling the number of alloys that could be tested before changing the electrodes in the deck.

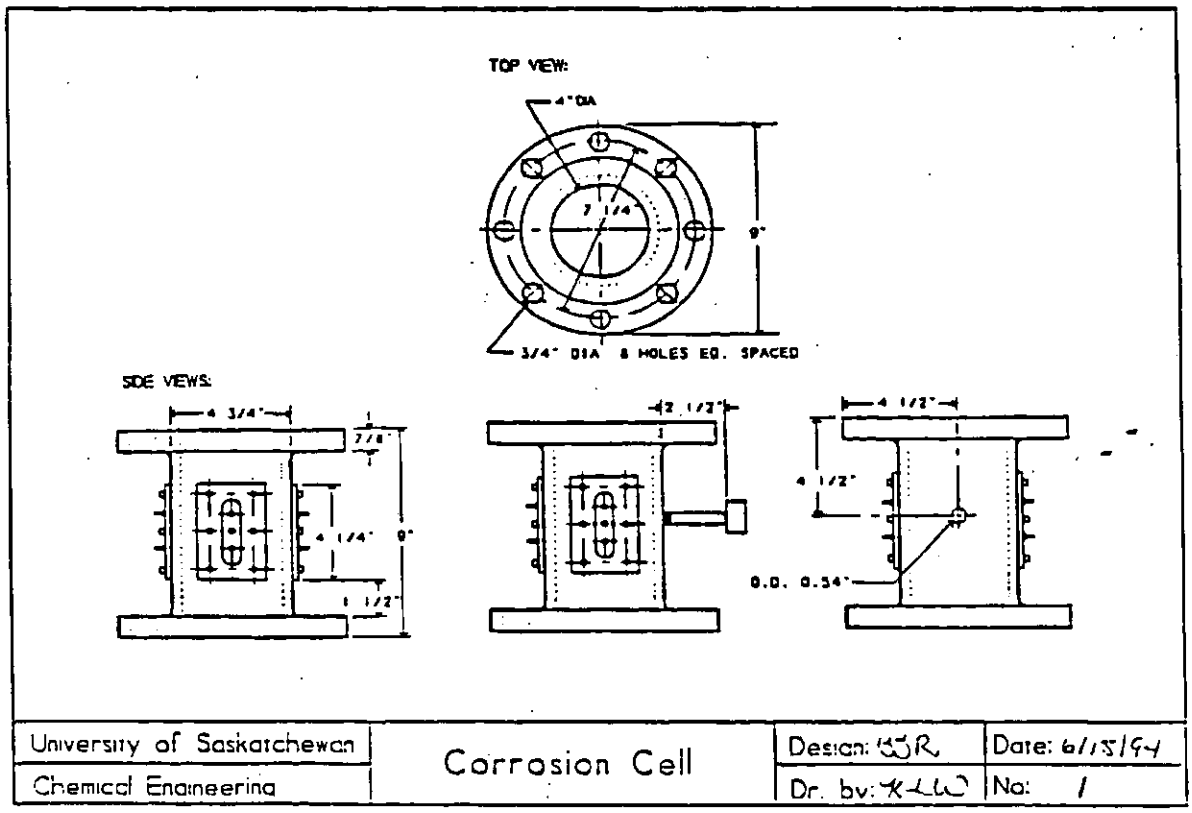

Figure 3.3 - Original Design by Brian J. Ritchie, Modifications by Craig E. Blackmore
Drawing by Kerry-Lynn Wersch

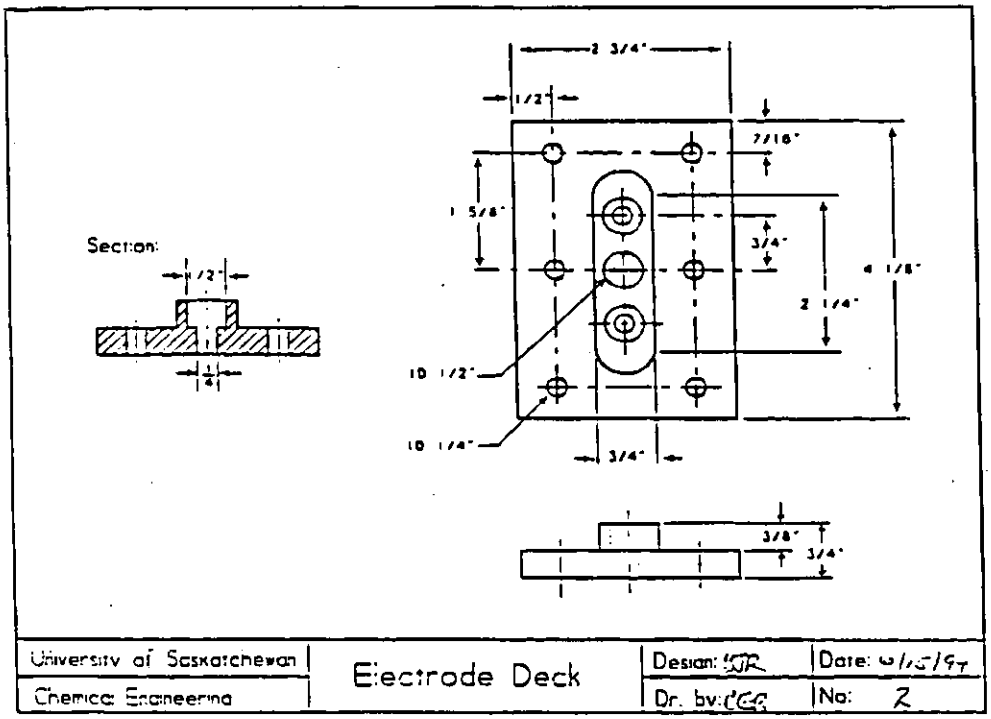

Figure 3.4- Original Design by Brian J. Ritchie, Modifications by Craig E. Blackmore
Drawing by Craig E. Blackmore

3.3.2. Experimental Conditions

3.3.2.1. Materials

The materials selected for tests in the pilot plant flow loop are shown in Table 3.3 with their component elements given in weight percentages. The weight percentages for these alloys are nominal compositions only. Specific alloy compositions for the electrodes used in these tests were not available. Alloy 20 and 2205 Duplex alloy were chosen to be tested in the full scale potash plant.

Table 3.3 Pilot Plant Alloy Compositions, wt%

Type	Alloy	Cr	Ni	Mo	N	Fe	C	Mn	Si	Cu	P	S
Nickel	C276	14.5-16.5	base	15.0-17.0	0	4.0-7.0	0.02 max	1.0 max	0.05 max	0	0.03 max	0.03max
Ans SS	316L	16.0-18.0	10.0-14.0	2.0-3.0	0	base	0.03 max	2.00 max	1.00 max	0	0	0
Duplex SS	2205	21.0-23.0	4.5-6.5	2.5-3.5	0.08-0.2	base	0.03 max	2.00 max	1.00 max	0	0	0
Duplex SS	Ferralinm	24.0-27.0	4.5-6.5	2.0-4.0	0.1-0.25	base	0.04 max	1.50 max	1.00 max	1.5-2.5	0.04 max	0.03 max
Duplex SS	3CR12	10.5-12.0	1.5 max	0	0	base	0.03 max	1.5 max	1.0 max	0	0.03 max	0.03 max
Cast SS	CD4	24.50-26.50	4.75-6.00	1.75-2.25	0	base	0.04 max	1.00 max	1.00 max	2.75-3.25	0.04 max	0.04 max
Cast SS	Alloy 20	19.00-22.00	27.5-30.5	2.0-3.0	0	base	0.07 max	1.50 max	1.50 max	3.00-4.00	0.04 max	0.04 max
Cast SS	Maxalloy II	14.0-18.0	0.5 max	2.3-3.5	0	base	2.8-3.6	0.5-1.5	1.0 max	1.2 max	0.1 max	0.05 max
Cast Iron	Ni Resist 1B	1.5-2.5	13.5-17.5	0	0	base	3.00 max	0.5-1.5	1.00-2.80	5.50-7.50	0	0
Cast Iron	Ductile Ni	1.75-2.75	18.0-22.0	0	0	base	3.00 max	0.70-1.25	1.50-3.00	0	0	0
Cast Iron	27% Cr	2.3-2.8	1.5 max	1.5 max	0	base	2.3-3.0	1.5 max	1.0 max	1.2 max	0.1 max	0.06 max
Cast Iron	#1 Ni Hard	1.4-4.0	3.3-5.0	1.0 max	0	base	3.0-3.6	1.3 max	0.3-0.8	0	0.3 max	0.15 max

3.3.2.2. Pilot Plant and Potash Mill Brines

The test spool was placed in a vertical line in the pilot plant flow loop where the brine flowed downward. The 101.6 mm (4") schedule 40 pipe carried the brine at 2.0-2.8m/s. Cyclic polarization and linear polarization experiments were performed on saturated KCl and 10% solids KCl at 85-90°C. The spool was in a horizontal 101.6 mm (4") pipe in the potash mill located between two crystallizers. The brine in the mill contained 24-28% solids and at 58-60°C, flowing at 3.9-4.2m/s. Both linear

and cyclic polarization techniques were used on the alloys tested in the mill. The list of alloys examined in the pilot plant and potash mill includes austenitic stainless steels, duplex steels, stainless and non stainless cast irons, making a selection different from the alloys studied in the laboratory.

3.3.3. Experimental Procedure

The experiments performed at the pilot plant were executed as follows: Once the electrode decks were in place and the flow loop had stablized at the desired temperature and velocity, the polarization resistance or cyclic polarization routine could be initiated on the Gamry™. At least thirty minutes elapsed after a routine to allow the electrodes to recover stable passivation before performing the next test.

3.4. Test Routines

3.4.1. Cyclic Polarization

Important information on localized corrosion is derived from the cyclic polarization test which acquires potential versus current data. Increasing the potential across a passivated electrode until localized corrosion begins allows one to pinpoint the potential at which pits initiate. This is the breakdown or pitting potential, E_{np}, as seen in Figure 3.5. The current density, *i*, will be low until the E_{np} is reached, and then it will dramatically increase as the pitting reactions begin, and electrons are more freely transferred from the electrode. Raising the potential will increase *i* as the pits propagate and grow larger. More pits initiate under these conditions. If the potential

is reduced, the current density does not follow the same pattern back as the pattern it followed when the potential was increasing. The current density is higher than before at the same potential. This creates a hysteresis loop as log(i) eventually returns to the low value where it began the experiment. The higher current density can be attributed to pits already initiated which continue to propagate and create current. No new pits nucleate in this loop region, but localized corrosion will continue to some extent. The pits repassivate, and the current density drops off, closing the loop. No initiation or propagation takes place and the corrosion reactions slow to their previous rate. The potential where log(i) reaches previously low levels is the protective potential, E_{pp}. If E_{pp} is never reached in the sweep, the current will follow its previous path on the return sweep because no pits would have initiated and there would then be no possibility for propagation [6].

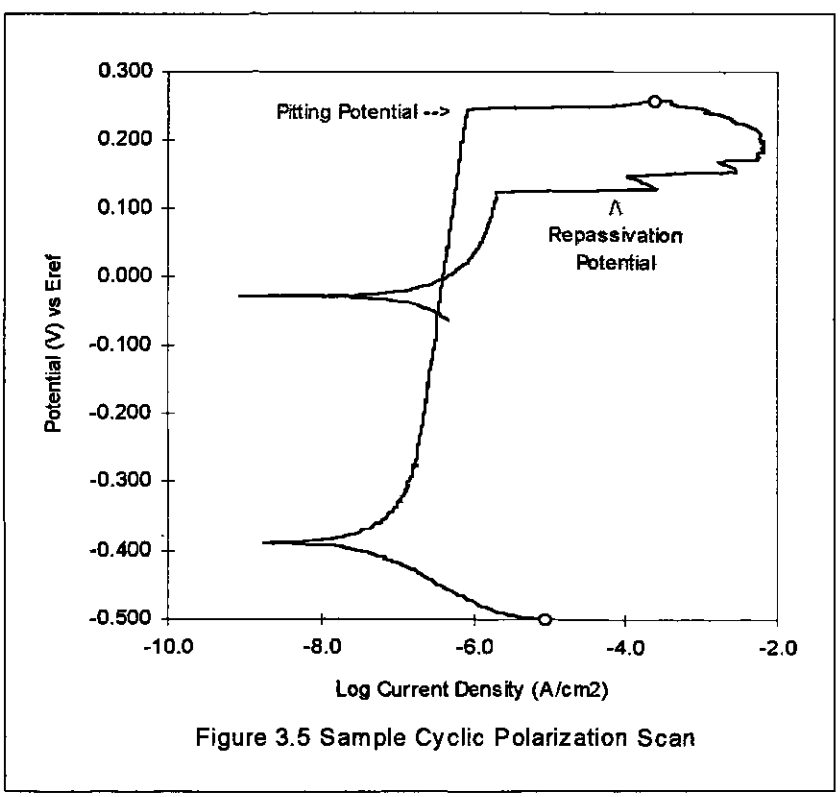

Figure 3.5 Sample Cyclic Polarization Scan

3.4.2. Linear Polarization

Linear polarization tests are used to find the polarization resistance of the material, which in turn is used to find the uniform corrosion rate. A linear polarization sweep increases potential over a small range near the open circuit potential of the system. The open circuit potential is ideally equivalent to the corrosion potential. When plotted on a current versus voltage graph, the curve is approximately a straight line with a slope giving the polarization resistance. An approximation of the Stern-Geary equation which represents a corroding system yields the following equation [21].

$$I_{corr} = \left[\frac{1}{R_p}\right]\left[\frac{b_a b_c}{2.303(b_a + b_c)}\right] \tag{3.2}$$

where I_{corr} is the corrosion current
R_p is the polarization resistance
b_a is the anodic Beta coefficient
b_c is the cathodic Beta coefficient

The beta coefficients come from the Tafel slopes of the anodic and cathodic reactions. The Tafel slopes are the slopes of the lines generated by a potential sweep when plotted on a potential versus log current density graph.

Chapter 4. Results

4. 1. Laboratory Results

The cyclic polarization experiments performed on rotating electrodes, as detailed in Chapter 3, yielded pitting potentials for each alloy over a range of temperatures. By plotting these potentials against the temperature, alloys with more stable passive layers and better resistance to the onset of localized corrosion can be visually identified. By determining pitting potentials at specific temperatures and plotting them against Localized Corrosion Resistance Indexes for the alloys, the validity of existing indexes can be verified or improved. As the tests used a simulated brine made from laboratory reagents, results using 316L stainless steel in brines from potash mills were also included.

4.1.1. Pitting Potential vs. Temperature

Figure 4.1a shows the experimental results which indicate that 254SMO gives superior protection over all the alloys tested. The 2205 duplex and 904L have comparable behavior, and are secondary in protection only to 254SMO. It should be noted that 2205 did not break down at 30°C or lower temperatures. The 316L clearly offers the best protection of the remaining alloys. Figure 4.1b gives a closer portrayal of the overlapping trends of these alloys. At lower temperatures, less than 50°C, 304L and 304LN are superior to 316LN, but the trend reverses at temperatures above

50°C. The 2304 duplex is the next best alloy to 316LN. The 304LN is slightly better than 304L at temperatures below 70°C. At and above 70°C, 304LN, 304L, 347ss and 17-4PH have indistinguishable degrees of resistance. CD4-MCu had a curious trend, having less resistance to localized corrosion than 304L at temperatures below 55°C, having equivalent resistance between 55°C and 65°C, and having more resistance at temperatures above 65°C. CN7M did not decrease in resistance with increasing temperature as dramatically as the other alloys. At about 50°C, CN7M had a resistance comparable to 446ss, but it dropped so little in resistance that it becomes comparable to 2304 duplex by 90°C. The ferritic stainless steels lost their passivity at lower potentials than the rest of the alloys. The 446ss was notably less resistant to localized corrosion above 50°C. As can be seen in Figure 4.1a, 430ss had far less resistance than any of the other alloys.

The testing indicates that under these conditions, 316L had a barely passable performance, and only 904L, 2205, and 254SMO have adequate resistance to localized corrosion.

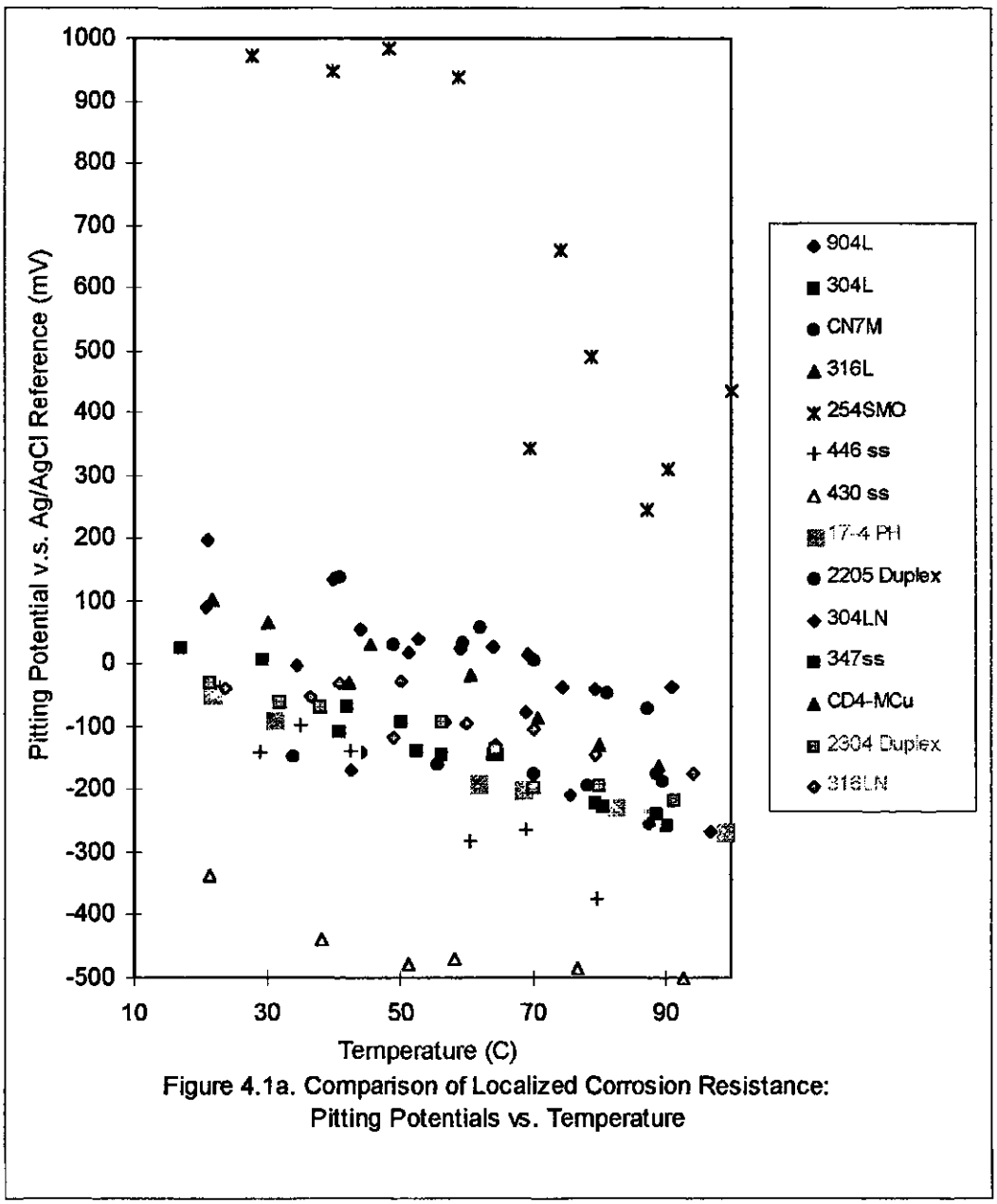

Figure 4.1a. Comparison of Localized Corrosion Resistance: Pitting Potentials vs. Temperature

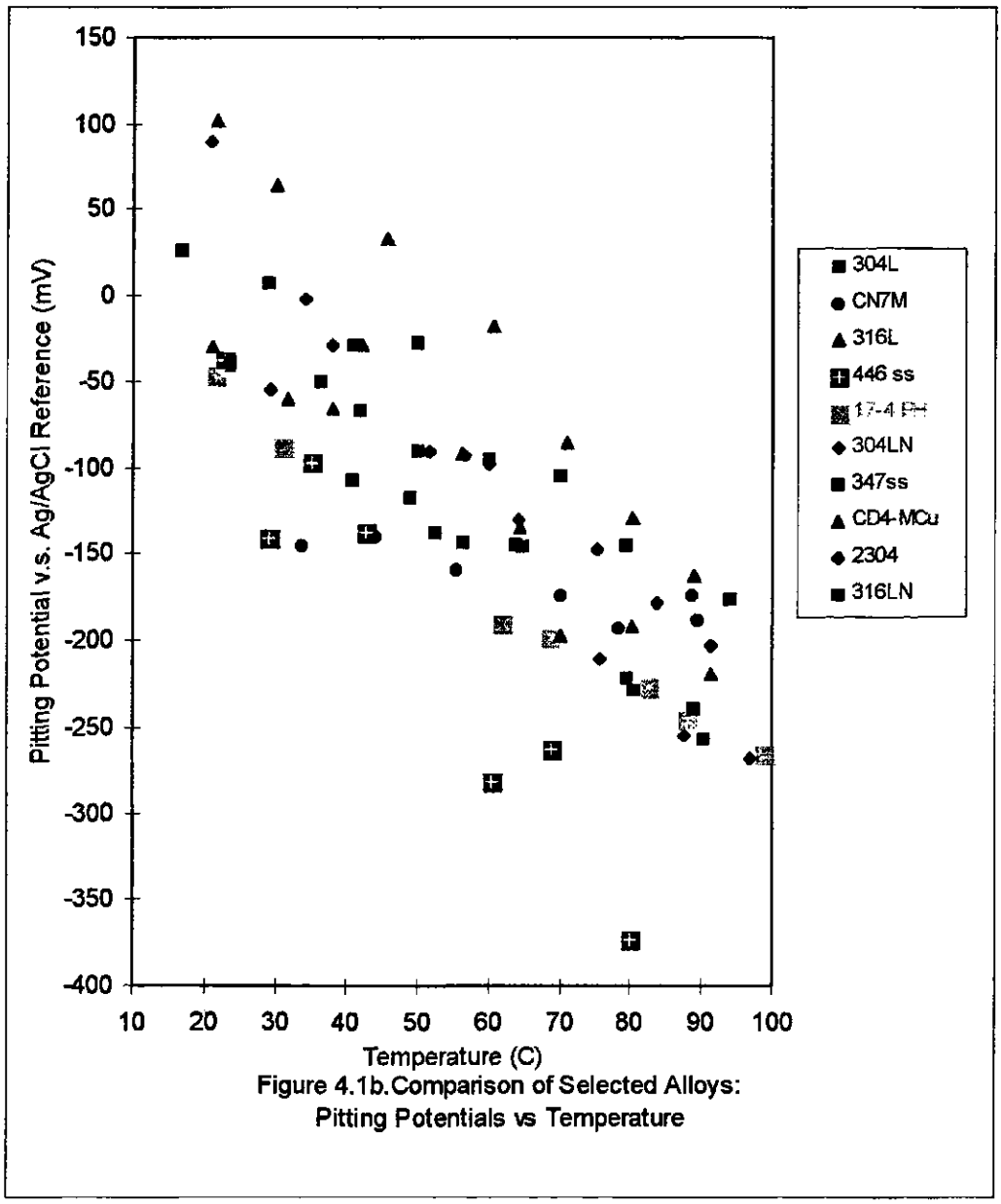

Figure 4.1b.Comparison of Selected Alloys:
Pitting Potentials vs Temperature

4.1.2. Pitting Potential in Plant Brines

The simulated brine was prepared with the quantity of each constituent salt being an average taken from composition reports on brines from mills around Saskatchewan. To verify that the simulated brine was indeed representative of actual mill brines, the 316L electrode was tested in three samples of brines taken from mills at Cory, Viscount and Vanscoy. Figure 4.2 shows the difference in pitting potentials

for each brine. It should be noted that the brines collected at Viscount and Vanscoy were not saturated at these temperatures. The plant brines promote localized corrosion over the simulated brine to a small degree. The plant brines themselves are comparatively close in their effect on pitting potentials. The simulated brine approaches the plant brine at higher temperatures which are the more critical conditions. Figure 4.3 compares the cyclic polarization curves themselves, and supports the use of the simulated brine as an average of typical mill brines.

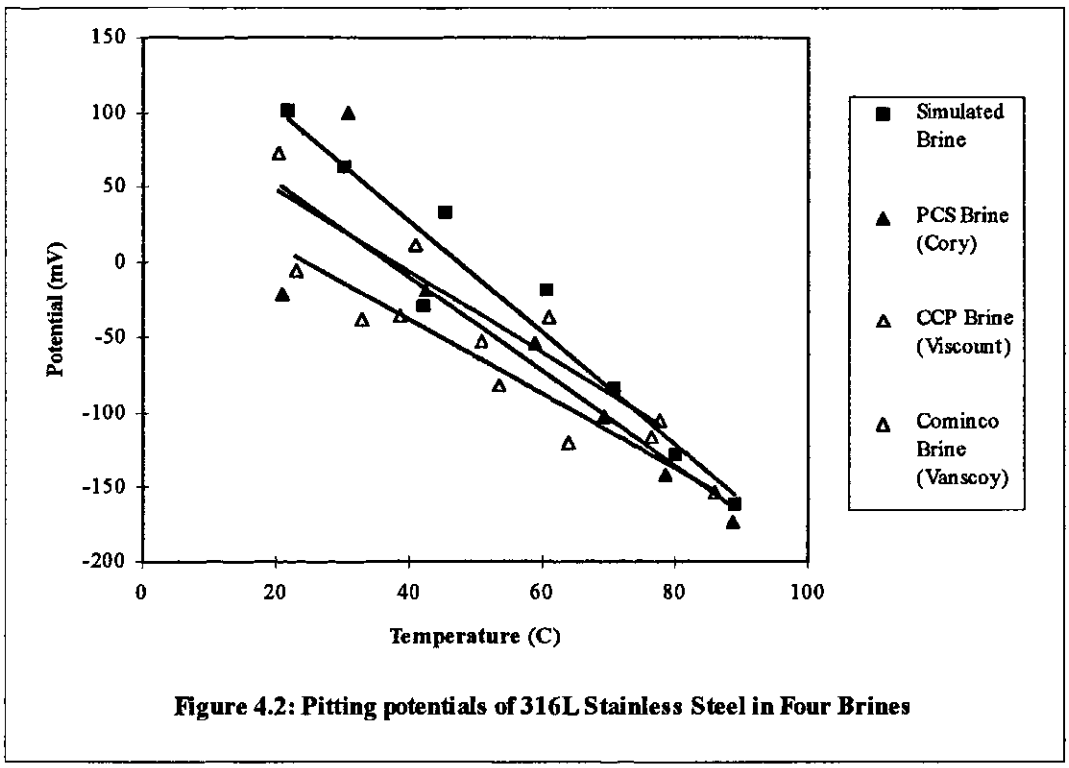

Figure 4.2: Pitting potentials of 316L Stainless Steel in Four Brines

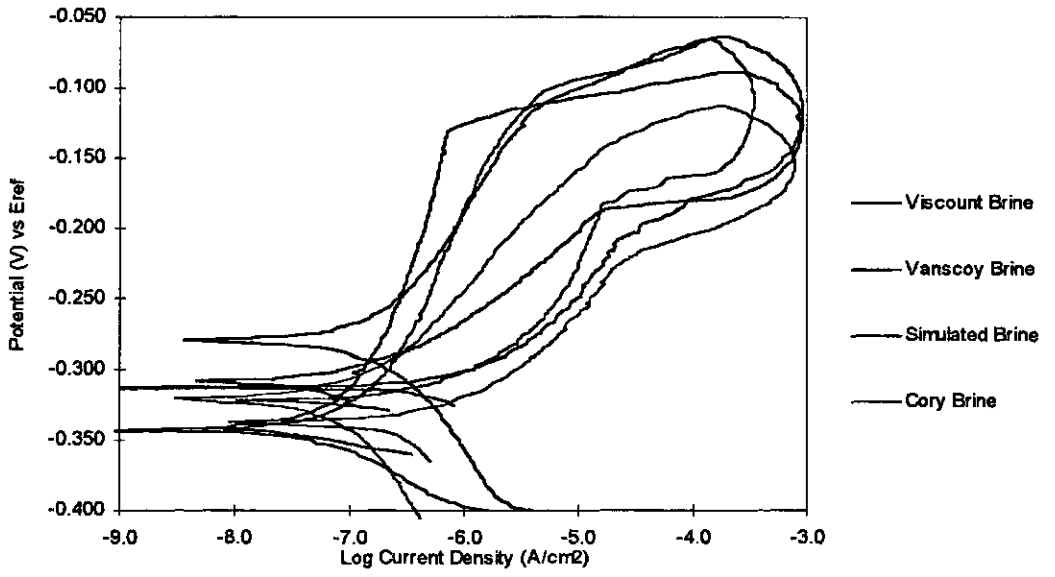

Figure 4.3 Comparison of Simulated Brine to Mill Brines at 80C

4.2. Pilot Plant and Potash Mill Experiment Results

The compositions of the alloys tested in the pilot plant flow loop are shown in Table 3.3.

4.2.1 Uniform Corrosion Rates.

The uniform corrosion rates are shown in Table 4.1. As would be expected the alloys that passivated had a much smaller corrosion rate than the alloys that remained in the active state. The corrosion rates for the passive alloys varied from <0.01 mm/year, with C-276 to 0.16 mm/year with the 316L stainless steel. The uniform corrosion rates for the active metals were much higher as would be expected. In practice these corrosion rates would be much lower as rust films develop. The alloy that was identified as "27% Chrome" in the supplier's data sheet in fact has 2.7%

chromium by weight as shown in the composition section on the same data sheet. As expected with this low chromium content the alloy did not passivate. Alloy 20 exhibited both active and passive behavior in the 10wt% solids solution.

Table 4.1 Uniform Corrosion Rates

Alloy	Corrosion Rate/(mm/year)	Solution
Passive		
C276	0.00	KCl, saturated,85-90 C
C276	0.00	
C276	0.00	
Ferrallium	0.01	
Alloy 20	0.04	
Ferrallium	0.04	
Ferrallium	0.04	
Alloy 20	0.07	
Alloy 20	0.08	
2205	0.08	
2205	0.10	
316L	0.16	
Not Passive		
Ni Resist 1B	0.74	KCl, saturated,85-90 C
Ni Resist 1B	0.88	
Ni Resist 1B	0.91	
Ni Resist 1B	0.91	
Ductile Ni	1.56	
CD4	1.72	
Ductile Ni	2.32	
Ductile Ni	2.50	
Passive		
2205	0.00	KCl, 10% solids, 85-90 C
Ferralium	0.01	
316L	0.01	
Ferralium	0.02	
2205	0.04	
CD4	0.05	
316L	0.06	
Alloy 20	0.07	
Alloy 20	0.08	
Not Passive		
27% Chrome	0.40	KCl, 10% solids, 85-90 C
Ni Resist 1B	0.83	
3CR12	0.83	
3CR12	1.83	
#1 Ni Hard	2.34	
Alloy 20	4.32	
27% Chrome	4.93	

Notes: 1. The alloy named '27% Chrome' actually contains only 2.7% Cr.
2. The corrosion rates of the non-passive alloys may be expected to decrease as a rust film develops.

4.2.2. Pitting Potentials

The results of the cyclic polarization tests are shown in Table 4.2.

Table 4.2 Localized Corrosion Tests

Alloy	Localized Corr Resistance Index= (%Cr +3.3%Mo +16%N - 0.33%Ni) low	high	Pitting Potential(V)	Epp (V)	Enp-Epp
Pilot Plant: saturated KCl, 85-90 C					
Passive					
C276	45.4	57	0.81	0.72	0.09
C276	45.4	57	0.60	0.59	0.01
2205	28.58	36	0.57	0.28	0.29
2205	28.58	36	0.52	0.26	0.26
Ferralium	30.25	43	0.35	0.14	0.22
Alloy 20	16.45	24	0.25	-0.05	0.30
316L	18.4	25	0.21	0.06	0.16
Alloy 20	16.45	24	0.18	0.00	0.17
Alloy 20	16.45	24	0.17	-0.01	0.18
316L	18.4	25	0.14	0.01	0.13
Non Passive					
Ni Resist 1B	-3.75	-2	no loop	no pass	no loop
Ductile Ni	-4.85	-3	no loop	no pass	no loop
Pilot plant:10%oversaturated KCl, 85-90 C					
Passive					
C276	45.4	57	0.60	0.60	0.00
Ferralium	30.25	43	0.36	0.15	0.21
2205	28.58	36	0.22	0.09	0.13
CD4	28.475	33	0.21	0.00	0.22
Alloy 20	16.45	24	0.17	0.03	0.14
316L	18.4	25	0.16	0.04	0.13
Alloy 20	16.45	24	0.13	0.03	0.10
Alloy 20	16.45	24	0.13	0.00	0.13
316L	18.4	25	0.11	-0.03	0.14
3CR12	10.05	12	0.03	-0.10	0.13
Non Passive					
Alloy 20	16.45	24	no loop		
Maxalloy II	21.44	29	no loop		
27% Chrome	6.8	7	no loop		
#1 Ni Hard	3.2	6	no loop		
Ni Resist 1B	-3.75	-2	no loop		
Cory Mill:24-28 wt%solids, 58-60 C					
2205	28.58	36	0.35	0.05	0.31
2205	28.58	36	0.34	0.10	0.24
Alloy 20	16.45	24	0.20	0.02	0.18

Note that the potentials are with reference to a stainless steel electrode at the same temperature as the working electrode.

The nickel alloy C-276 and the two duplex stainless steels Ferralium and 2205 Duplex rank the highest. Alloy 20 did not passivate in one test in the 10 wt.% solids solution in the pilot plant but did passivate in three other tests under the same conditions. Maxalloy contains 14-18% Cr and it is surprising that this alloy did not passivate.

Chapter 5. Discussion of Results

5.1. Reproducibility of Results

The electrochemical experiments are easily reproduced and give consistent results. Figure 5.1 compares two sets of data obtained from cyclic polarization scans of 904L in the glass cell immersed in deaerated simulated brine. The scans were performed one week apart after the 904L electrode had been removed from the cell, repolished to 600 grit, and reimmersed for the second scan. The pitting potentials and repassivation potentials taken from each scan are near enough to cause no concern for the reproducibility of the experiments.

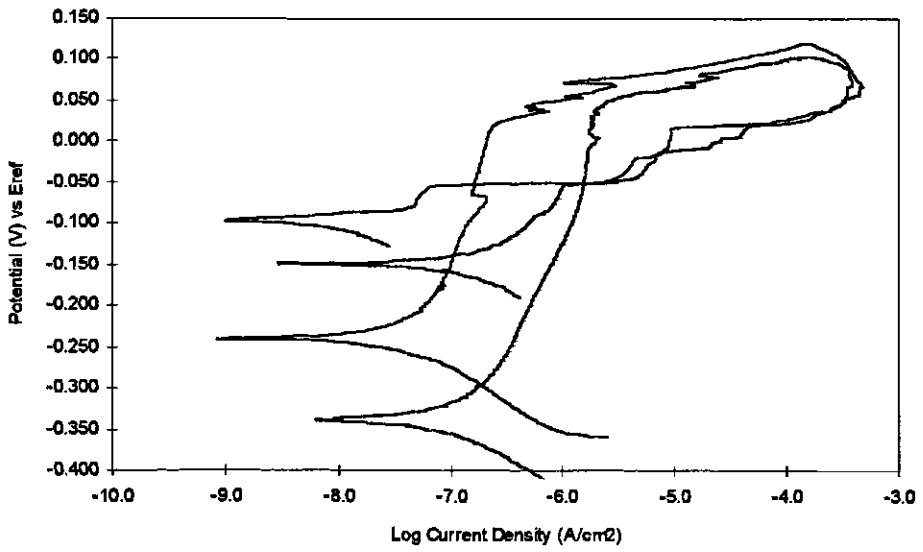

Figure 5.1 Reproducability of Cyclic Polarization Curves: 904L steel at 50 C

5.2. The Localized Corrosion Resistance Index

The relationship between the Localized Corrosion Resistance Index, (LCRI), Cr%+3.3(Mo%)-0.33(Ni%)+16(N%), and the true resistance of the alloys under examination was investigated by plotting the pitting potentials at 40, 60, and 80°C against the LCRI value of the alloy. Figure 5.2 gives an overall look at the materials studied. Figure 5.3 excludes the alloys that the LCRI does not accurately predict.

To quantify the validity of the LCRI, linear regressions were performed on each series. Plots of several resistance indexes were regressed with the results reported in Table 5.1. Examples of these plots, Figure 5.4 was included for LCRI5 and LCRI7 which examines the molybdenum factor, and Figure 5.5 was included for LCRI9 and LCRI11 which had the best regressions. Tables 5.2a and 5.2b give the LCRI values for all the alloys. The ranking of the alloys is given by order of LCRI value in Table 5.2a and LCRI11 value in Table 5.2b.

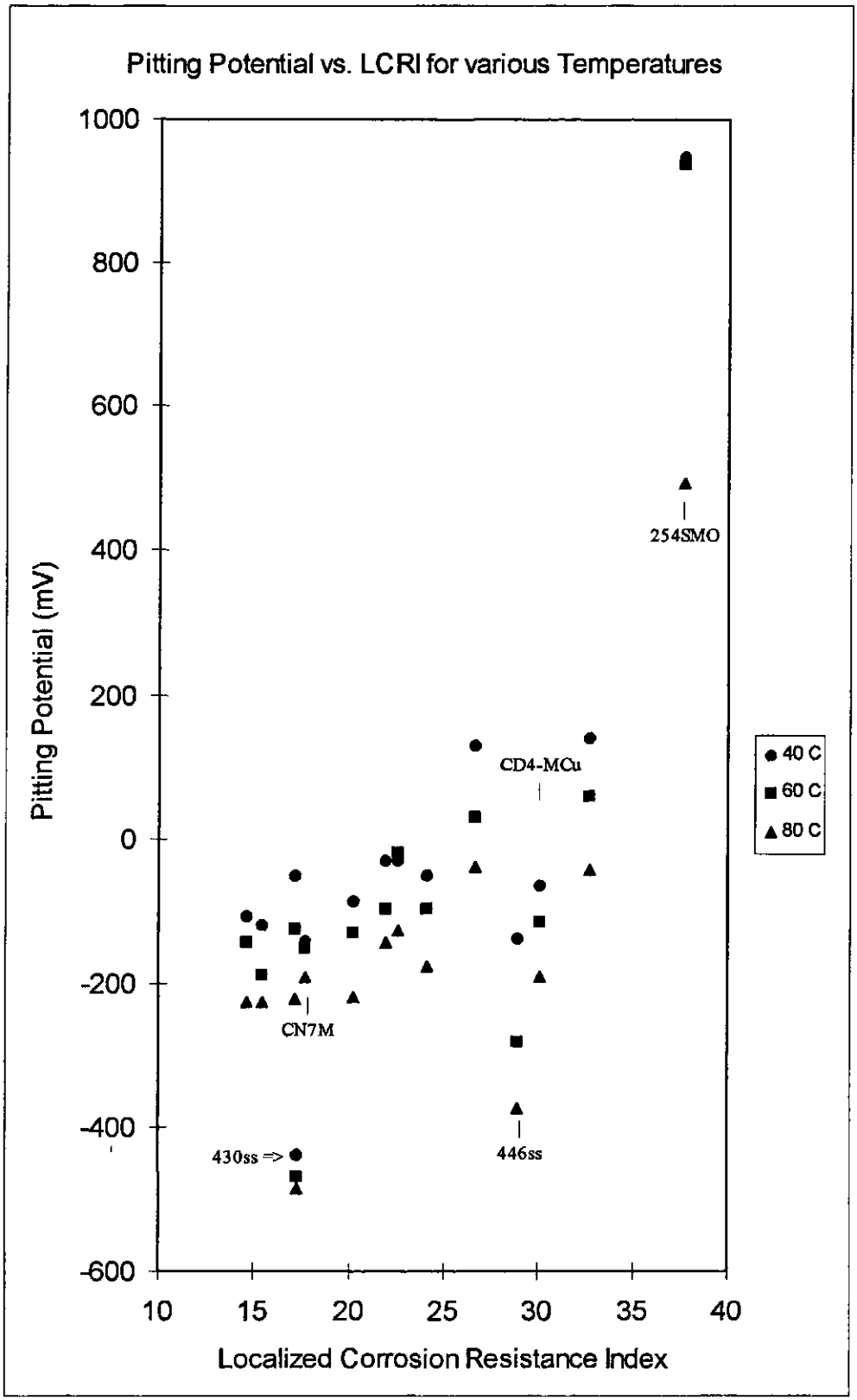

Figure 5.2 Master Plot of All Alloys Examined

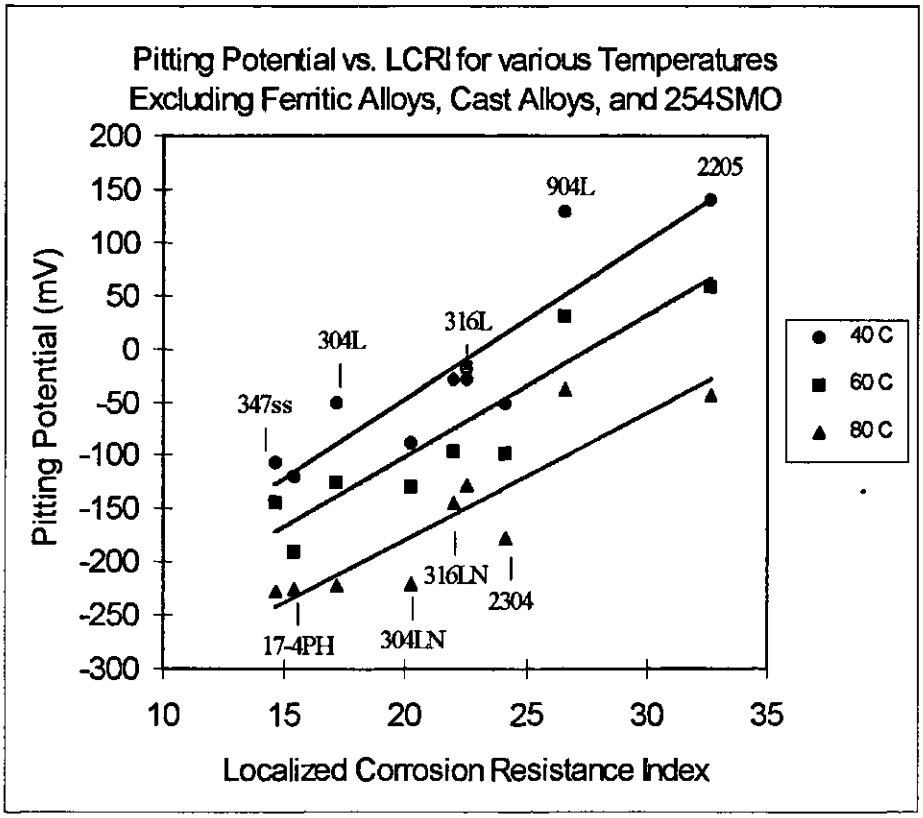

Figure 5.3 Regression Trends of LCRI Sensitive Alloys

Table 5.1 Accuracy of Selected Localized Corrosion Resistance Indexes

		Linear Regression - R squared values		
Index#	Index Formula	40C	60C	80C
LCRI	Cr+3.3*Mo-0.33*Ni+16*N	0.797	0.786	0.800
LCRI2	Cr+3.3*Mo-0.33*Ni+30*N	0.720	0.763	0.720
LCRI3	Cr+3.3*Mo-0.33*Ni	0.874	0.871	0.882
LCRI4	Cr+3.3*Mo+16*N	0.903	0.912	0.922
LCRI5	Cr+3.3*Mo	0.925	0.908	0.949
LCRI6	Cr	0.343	0.341	0.238
LCRI7	Cr+4.1*Mo	0.923	0.906	0.965
LCRI8	Cr+4.1*Mo+6*N	0.923	0.914	0.963
LCRI9	Cr+4.1*Mo+6*N-0.1*Ni	0.927	0.922	0.964
LCRI10	Cr+4.1*Mo-0.14*Ni	0.933	0.920	0.971
LCRI11	Cr+4.1*Mo-0.14*Ni+6*N	0.926	0.922	0.962
LCRI12	Cr+3.3*Mo+2*N	0.925	0.910	0.948

Table 5.2a. Localized Corrosion Resistance Index Values for Each Alloy by the Indexes included in Table 6

Alloy	LCRI	LCRI2	LCRI3	LCRI4	LCRI5	LCRI6	LCRI7	LCRI8	LCRI9	LCRI10	LCRI11	LCRI12
347 ss	14.6	14.6	14.6	17.9	17.9	17.1	18.1	18.1	17.1	16.7	16.7	17.9
17-4 PH	15.4	15.4	15.4	16.8	16.8	15.4	17.1	17.1	16.7	16.5	16.5	16.8
304L	17.1	18.0	16.1	20.0	19.0	18.2	19.2	19.6	18.7	18.0	18.4	19.1
430 ss	17.2	17.7	16.6	17.3	16.7	16.6	16.8	17.0	17.0	16.7	16.9	16.8
CN7M	17.7	17.7	17.7	27.2	27.2	20.0	29.0	29.0	26.1	24.9	24.9	27.2
304LN	20.2	21.9	18.2	23.1	21.1	19.8	21.4	22.2	21.3	20.2	21.0	21.4
316LN	21.9	23.6	20.0	25.3	23.4	16.5	25.0	25.8	24.7	23.6	24.3	23.6
316L	22.5	23.7	21.2	26.4	25.0	17.5	26.9	27.4	26.2	25.2	25.7	25.2
2304	24.1	25.8	22.2	25.6	23.7	22.5	23.9	24.7	24.2	23.3	24.0	23.9
904L	26.6	26.6	26.6	34.5	34.5	20.3	38.0	38.0	35.6	34.6	34.6	34.5
446 ss	28.9	31.4	26.0	28.9	26.0	26.0	26.0	27.1	27.1	26.0	27.1	26.3
CD4-MCu	30.0	30.0	30.0	31.7	31.7	25.5	33.2	33.2	32.7	32.5	32.5	31.7
2205	32.7	34.8	30.3	34.5	32.1	22.2	34.5	35.4	34.8	33.7	34.6	32.4
254SMO	37.7	40.5	34.5	43.6	40.4	20.1	45.3	46.5	44.7	42.8	44.0	40.8

Table 5.2b. Comparison of Alloy Indexes LCRI11, LCRI, and LCRI9

Alloy	LCRI11	LCRI	LCRI9
17-4 PH	16.5	15.4	16.7
347 ss	16.7	14.6	17.1
430 ss	16.9	17.2	17.0
304L	18.4	17.1	18.7
304LN	21.0	20.2	21.3
2304	24.0	24.1	24.2
316LN	24.3	21.9	24.7
CN7M	24.9	17.7	26.1
316L	25.7	22.5	26.2
446 ss	27.1	28.9	27.1
CD4-MCu	32.5	30.0	32.7
904L	34.6	26.6	35.6
2205	34.6	32.7	34.8
254SMO	44.0	37.7	44.7

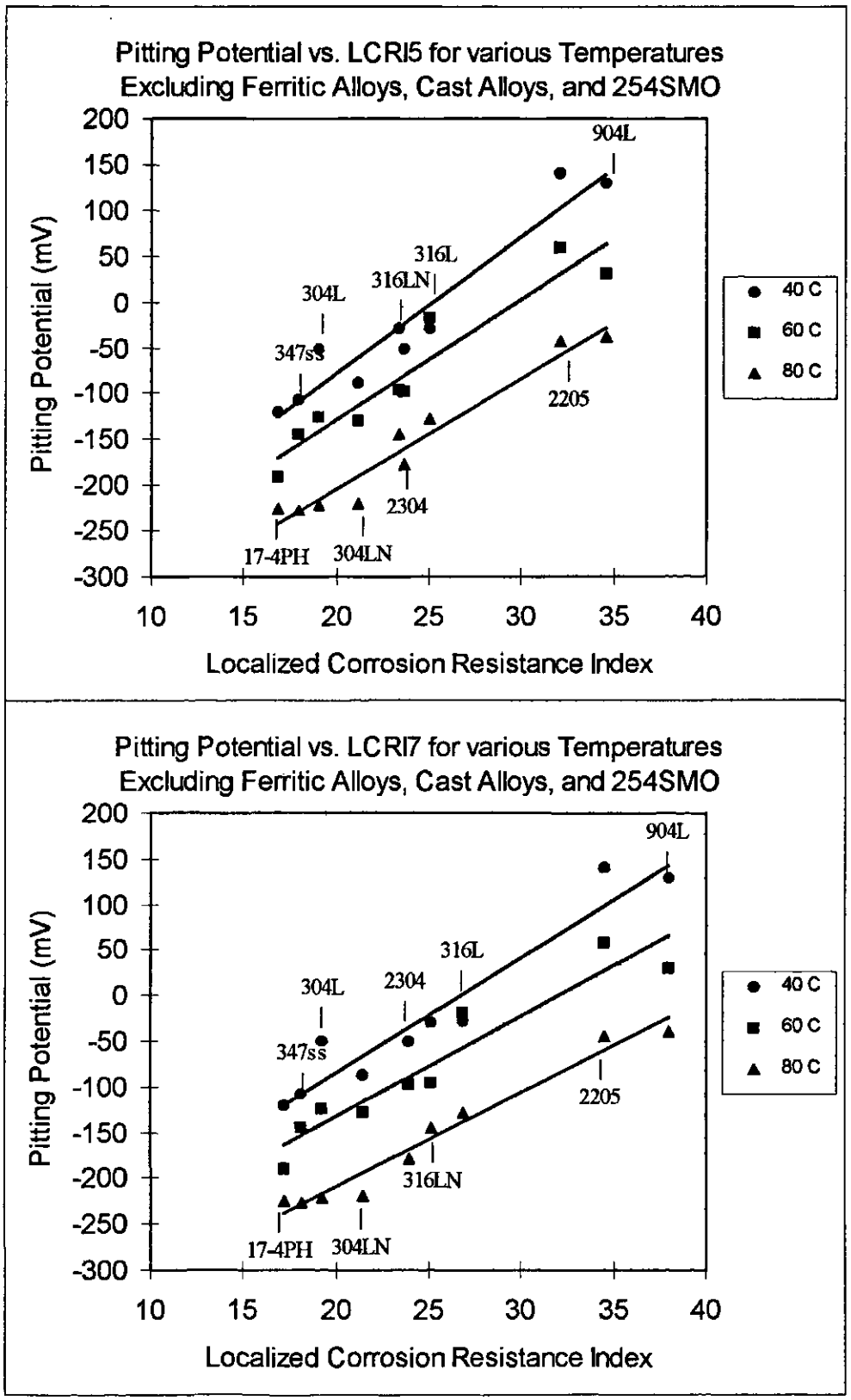

Figure 5.4 LCRI5 and LCRI7 Regressions,
LCRI5 = Cr%+3.3Mo% , LCRI7 = Cr%+4.1Mo%

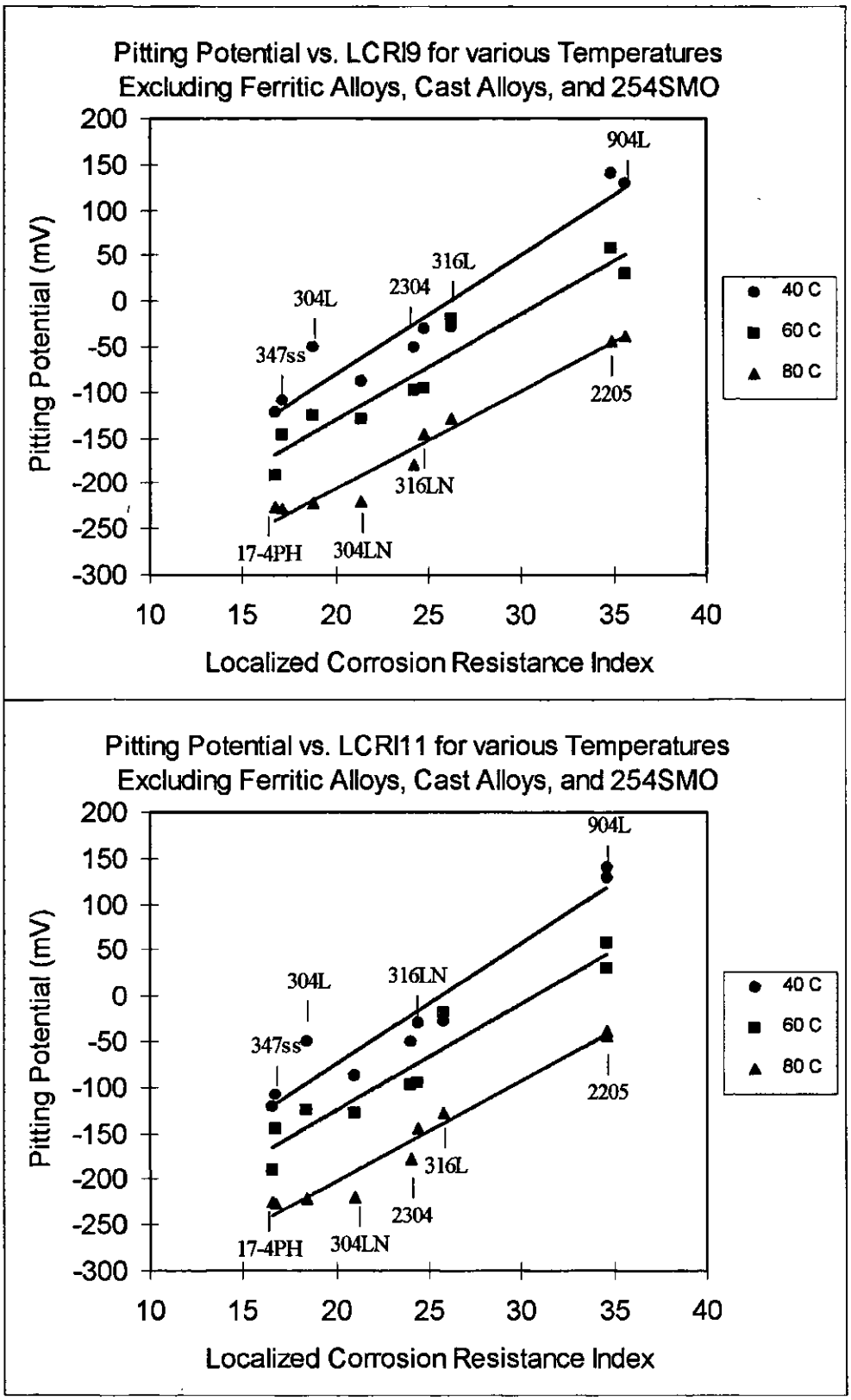

Figure 5.5 Regressions:
LCRI9 = Cr%+4.1Mo%-0.10Ni%+6N%
LCRI11 = Cr%+4.1Mo%-0.14Ni%+6N%

Table 5.1 contains the R^2 values for linear regressions performed on the alloys excluding 254SMO, CD4-MCu, CN7M, 430ss and 446ss. The LCRI2 was derived from the practice of doubling the nitrogen factor for duplex stainless steels as outlined in Bernhardsson [16]. As can be seen in Table 5.1, the data did not support this index. Calculating LCRI2 for only the duplex steels and combining them with the LCRI data for the rest of the alloys yields poorer results. LCRI2 is therefore not recommended.

By removing terms for nitrogen and nickel from the LCRI, formulas for LCRI3 and LCRI4 were created. LCRI4 is in fact the earlier predecessor to the LCRI and is currently in widespread use. An examination of LCRI3 and LCRI4 regressions shows the greater influence of the nitrogen term compared to the nickel term. Simplifying even further, the localized corrosion index, Cr%+3.3Mo%, is revealed. Denoted LCRI5, it provides an accurate portrayal of the behavior of the alloys.

The most linear relation obtained thus far was with LCRI5. Nitrogen and Nickel were not accounted for in LCRI5. The next step was to build an index that included these elements and maintained the highest possible linearity. The molybdenum term was reworked to create LCRI7. Figure 5.4 compares the results graphically. The improvement in the regressions is relatively minute, but the more appropriate ranking of 316LN as superior to 2304 gives credibility to LCRI7. Nitrogen and then nickel terms were added onto LCRI8 and LCRI9 in that order. Each addition improved the correlation slightly. LCRI9 had the best regression of all the indexes. LCRI11 was created to determine if a better index could be assembled

from the optimum nickel term added to LCRI7 (found trough LCRI10). The LCRI11 regressions were almost as good as LCRI9's. LCRI11, however, ranks 904L and 2205 Duplex as identical while LCRI9 predicts 904L should have a noticeably superior resistance not seen in the data (see Figure 4.1b). LCRI11 fits the gathered data and is just as good of an index as those being currently used in industry.

5.2.1. Ferritic Stainless Steels and Cast Corrosion Resistant Stainless Steels

When considering the validity of the Localized Corrosion Resistance Index (LCRI), stark differences are seen between the austenitic and ferritic alloys. Nadezhdin and Wensley [1] used only austenitic and duplex stainless steels to gather data for the formulation of the LCRI. It can be seen in Figures 4.1a and 5.2 that the ferritic stainless steels 430 and 446 were much less resistant than their LCRI values indicate. Ferritic stainless steels should not use existing corrosion resistance indexes as guides for their behavior in high chloride environments. Correction factors that bring the ferritic steels into the LCRI ranking as it now exists are impractical. The 430 ss would have a negative index value, and 446ss has a large dependence on temperature. A new correlation for ferritic steels should be formulated. With data on only two ferritic steels, a new correlation was beyond the scope of this study.

Cast corrosion resistant stainless steels also posed a problem for the LCRI. The CD4-MCu behaved very poorly considering the quantity of chromium it contains, and does not correlate with the data for the other austenitic stainless steels. The CN7M appeared to be within the correlation for the LCRI, but Table 5.3 demonstrates that, without CN7M, better regressions are formed for LCRI4 and

LCRI5; indexes that do not account for nickel compositions. Given the heterogeneous nature of the alloy surface from the casting process, the cast alloys were removed from further regressions of the indexes. A rough estimate that could be used to rank the cast alloys along with the other alloys was indicated by Figure 5.2. The LCRI values for CD4-MCu and CN7M multiplied by a factor of 0.75 would place these cast alloys roughly in the range of LCRI value that their behavior suggests. This could be extended to other cast alloys, but a more complete study of this class of materials should be performed to establish more accuracy in predicting their behavior.

Table 5.3 Comparison of Regressions of Corrosion Indexes to Evaluate the Applicability of CN7M

			Linear Regression - R squared values		
Index #	Index Formula	CN7M	40C	60C	80C
LCRI	Cr+3.3*Mo-0.33*Ni+16*N	INCLUDED	0.792	0.830	0.801
LCRI	Cr+3.3*Mo-0.33*Ni+16*N	EXCLUDED	0.797	0.786	0.800
LCRI2	Cr+3.3*Mo-0.33*Ni+30*N	INCLUDED	0.733	0.779	0.720
LCRI2	Cr+3.3*Mo-0.33*Ni+30*N	EXCLUDED	0.720	0.763	0.720
LCRI3	Cr+3.3*Mo-0.33*Ni	INCLUDED	0.842	0.868	0.884
LCRI3	Cr+3.3*Mo-0.33*Ni	EXCLUDED	0.874	0.871	0.882
LCRI4	Cr+3.3*Mo+16*N	INCLUDED	0.681	0.773	0.857
LCRI4	Cr+3.3*Mo+16*N	EXCLUDED	0.903	0.912	0.922
LCRI5	Cr+3.3*Mo	INCLUDED	0.641	0.720	0.845
LCRI5	Cr+3.3*Mo	EXCLUDED	0.925	0.908	0.949

5.2.2. Austenitic, Duplex, and Precipitation Hardened Stainless Steels

The austenitic alloys, duplex stainless steels, and 17-4PH steel were used to examine the indexes as detailed in Section 5.2. The 17-4PH has a martinsitic structure, but fits in well with the austenitic steels and was included in the LCRI evaluations. The 254SMO was excluded from the regressions because of its dramatically resistant behavior relative to its index values. The behavior of this alloy would still be predicted to be extreme resistance to localized corrosion based on the LCRI number. The exclusion does not harm the validity of the evaluations. The index created by this study, LCRI11, classifies 254SMO as more passive compared to the other alloys than the LCRI would classify it. This indicates that the LCRI11 should be a better index for identifying alloys which passivate this strongly.

The austenitic-ferritic duplex steels, 2205 and 2304, did not meet the expected resistance given the LCRI values, but were not as seriously displaced from the expected behavior as the ferritic steels. The competing factors of structure and chromium content in duplex stainless steels as outlined in Chapter 2 make predicting the cause of corrosion resistance difficult when examining these alloys, but the LCRI and LCRI11 indicate that corrosion indexes are accurate enough for use with duplex alloys.

5.2.2.1. Component Effects

The indexes are based on factoring in the value of a component element relative to the value of chromium regarding the resistance of an alloy to localized corrosion. Molybdenum is the most important element next to chromium due to its

effect in strengthening the passive layer. The LCRI may rate molybdenum below its actual influence. The LCRI11 was formulated with a +4.1(Mo%) term as opposed to the LCRI's +3.3(Mo%) term. Both terms bring the index values into reasonable ranges for accurate comparison and ranking of alloys. There is no disputing the positive effect of molybdenum.

Nitrogen was found to have less influence in the LCRI11 than the original LCRI allotted. The factors rated the nitrogen percentage at 6 and 16 respectively. When creating the nitrogen term for LCRI12, based on LCRI5 (Cr%+3.3Mo%) the nitrogen factor was only 2. The most appropriate term for nickel was carefully determined. A better index (LCRI11) was obtained by considering the linearity of a Cr, Mo, N index (LCRI8) and a Cr, Mo, Ni index (LCRI10) separately rather than through attempts to add a nickel term to an existing Cr, Mo, N index. The end result was a factor for nickel weaker than in the original LCRI (-0.14 as opposed to -0.33), but still showing the negative influence the element has on the passivity of the alloy.

An attempt to include more elements in the index failed mainly because the regressions had a high degree of linearity with only the four terms. There was less room for improvement of the regressions, and the influence of the elements was difficult to detect. The LCRI has an adequate number of terms for differentiating the resistance of passive alloys with structures similar to those included in the study. The major contributing elements to the passivity of stainless alloys are addressed. Although the LCRI, as it currently exists, is sufficient in ranking and evaluating these alloys, the new LCRI11 developed from the experimental data would be

advantageous for use in the Potash Industry. It was developed under the high chloride conditions common in potash mills.

5.2.2.2. Temperature Effects

Figure 4.1a demonstrated the influence of temperature on the pitting potentials of the alloys examined. All alloys with the exception of CN7M experienced a noteworthy decrease in resistance with an increase in temperature. This was expected, but there was concern over differences and variations in the degree of loss of resistance among the alloys which could alter the ranking over the temperature range. Fortunately, this was not seen in the data. The alloys that crossed trends remained close enough that their resistance was effectively the same and would not interfere greatly with the LCRI. There was also concern over "critical pitting temperatures" that would show a steep drop in resistance over a short temperature range between two plateaus and where these critical temperatures may exist for different alloys. This type of trend was seen only in 254SMO which had a critical pitting temperature in the 70 to 80°C range. The pitting potentials for 254SMO were well above the rest of the alloys even at high temperatures, and there was no interference in the ranking of the alloys.

5.3. Pilot Plant and Potash Mill Electrode Deck Experiments

The pilot plant experiments gave a comparison of various alloys in a flow situation that was simulated by the rotating cylindrical electrode in the laboratory. The electrolyte solutions were different and the temperatures in the pilot plant were

kept to an extreme. Figure 5.6 displays the results of the cyclic polarization tests and shows that the LCRI is accurate in real flow conditions. The uniform corrosion rates were reasonable. The passive alloys had very low rates while the non-passive had much higher rates.

The potash mill experiments were performed chiefly to evaluate the electrochemical test equipment under mill conditions and supplement the pilot plant data. The Gamry™ CMS100 corrosion measurement system performed well in the potash mill giving stable cyclic polarization curves and data that compared well with the pilot plant results considering the differences in temperature.

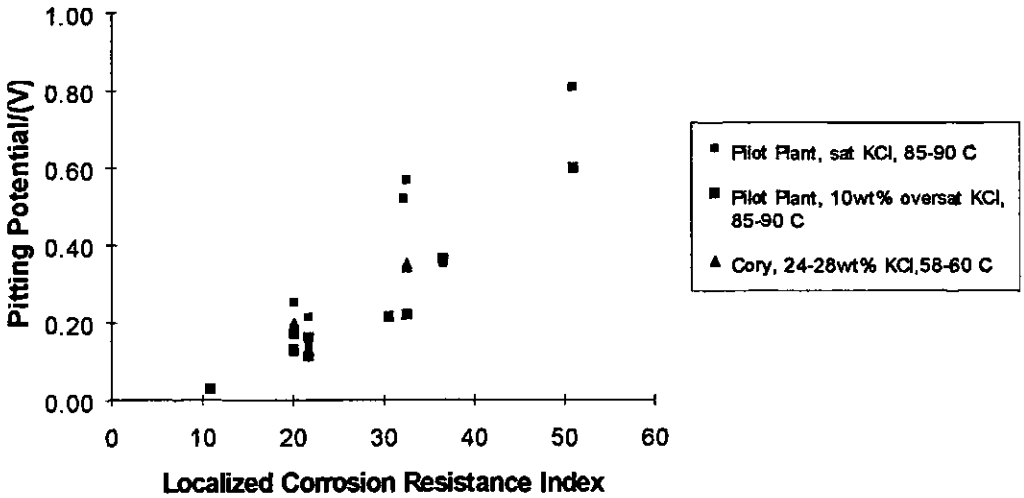

Figure 5.6 Pitting Potential (Compared to 316L Stainless Steel Eref) vs. Localized Corrosion Resistance Index

Chapter 6. Conclusions

1. The Localized Corrosion Resistance Index, Cr%+3.3(Mo%)-0.33(Ni%)+16(N%), by Nadezhdin and Wensley can adequately predict the resistance of passive alloys to pitting and crevice corrosion in high chloride environments as experienced in the potash industry. The experimental data in this study supported the LCRI in the laboratory, pilot plant flow loop, and full-scale potash mill. A single universal index that applies to all industrial conditions and types of alloy would not be as practical as a few more specified indexes used by individual industries.
2. The Gamry CMS100 Corrosion Measurement System™ is a reliable and efficient tool for performing electrochemical corrosion testing. The portability and durability allow for experimentation in areas less robust potentiostats would not be recommended. The test routines are convenient and offer suitable control over experiments with the option of programming personalized test routines.
3. The simulated brine mixture used in the laboratory glass cell approximates actual plant brines within an acceptable range. Actual brines may undermine passivity a little more readily than the simulated brine at lower temperatures. The brines tested in this study compared well to one another.

4. The Localized Corrosion Resistance Index **can not** be applied to ferritic stainless steels as it now exists. A new formula for ferritic steels would have to be created to compare the resistance of these alloys to the resistance of austenitic and duplex alloys. The ferritic alloys performed very poorly considering their chromium content. They did passivate, but pitted very readily.

5. Cast corrosion resistant alloys do not fit into the LCRI correlations. The cast alloys tested in this study showed consistently lower results than predicted by the LCRI. A rough comparison could be made if the LCRI value of the cast alloy were multiplied by 0.75 .

6. Duplex stainless steels fit into the LCRI correlation almost as well as austenitic alloys. The slight discrepancy can be explained by the austenitic-ferritic structure. The austenite loses some chromium to the ferritic phase. The less passive ferritic phase may be the anodic sites initiating pitting, or the weakened austenite could prove more susceptible. Given the poor performance of the ferritic alloys, the evidence appears to point to pits initiating in the ferritic phase even though that phase would have extra chromium. The superior performance of the duplexes compared to the ferritic alloys would then be due to the elevated chromium content.

7. Temperature has minimal effect on ranking alloys with the LCRI. The general trends of decreasing resistance to pitting with increasing temperature were similar for most of the alloys and did not interfere with the ranking.

8. The best elements to consider for the corrosion indexes are chromium, molybdenum, nitrogen, and nickel. The addition of other elements - carbon, silicon etc. do not increase the accuracy of the index significantly.

9. The experimental data supported the theories regarding the positive effect of nitrogen and the negative effect of nickel on resistance to localized corrosion. A new index was compiled, LCRI11, Cr%+4.1(Mo%)-0.14(Ni%)+6(N%). This index places more emphasis on the benefit of molybdenum and less emphasis on the effects of nickel and nitrogen.

10. Comparing the LCRI and LCRI11 linear regressions shows that LCRI11 gives significantly more linear values. Ranking of the alloys by the LCRI11 is more accurate and better accounts for anomalies like the high resistance of the 254SMO. This suggests LCRI11 allows for better prediction of high resistance alloys and should fit duplex alloys better than the LCRI. The LCRI11 was formulated using potash industry conditions, whereas the LCRI was formulated using pulp and paper conditions. The LCRI11 would be better than the LCRI for use by the potash industry.

Chapter 7. Recommendations

The electrochemical corrosion testing performed for this study provided precise data on the localized corrosion of the alloys tested. Additional investigation into the corrosion of these alloys employing long term corrosion experiments with artificial crevices on coupons in brine would be beneficial. There is potential to learn more about the corrosion of these alloys, especially the exact site of attack on duplex alloys.

A full study into the localized corrosion of ferritic alloys would yield the opportunity to create a new corrosion index specific to these alloys or to bring them into the LCRI ranking range. The suspicious behavior of the cast corrosion resistant alloys, CN7M and CD4-MCu, opens up another avenue for further investigation. These alloys may be unpredictable; if they prove to be predictable, they could more easily be incorporated into the rankings than the ferritic alloys.

The severe high chloride - elevated temperature environments encountered in the potash industry require attention to localized corrosion behavior to support material selection decisions and prevent costly losses to the industry.

References

[1] A. Nadezhdin and D.A. Wensley. "Composition Factors Affecting Resistance of Ni-Cr-Mo-N Alloys to Crevice Corrosion". Materials Performance, p. 57 (Nov 1992)

[2] J. Bockris and A. Reddy. Modern Electrochemistry, Vol. 2, p. 1318 (1970)

[3] M.A.C. de Castro and B.E. Wild. Corrosion, Vol. 35, p. 560 (1979)

[4] Z. Szklarska-Smialowska. Pitting Corrosion of Metals, 1st ed. National Association of Corrosion Engineers, p. 378 (1986)

[5] D. Choi and G.S. Was. Corrosion, Vol. 48, p. 292 (1992)

[6] J. Postlethwaite. Canadian Metallurgical Quarterly, Vol. 22, p. 133 (1983)

[7] Z. Szklarska-Smialowska. Pitting Corrosion of Metals, 1st ed. National Association of Corrosion Engineers, p. 394 (1986)

[8] J. Bockris and A. Reddy. Modern Electrochemistry, Vol. 2, p. 1318 (1970)

[9] K.J. Vetter and H.H. Strehblow. Localized Corrosion, NACE-3, p. 240 (1974)

[10] M.B. Ives and H.H. Strehblow. Corrosion Science, p. 317 (1976)

[11] M. Urgen and A.F. Cakir. Corrosion Science, Vol. 32, p. 841 (1991)

[12] G.C. Palit, V. Kain, and H.S. Gadiyar. Corrosion, Vol. 49, p. 977 (1993)

[13] A. Moskowitz, G.A. Saltzman, K.E. Pinnow, and L.S. Redmerski. "Influence of Residual and Minor Elements on the Pitting and Atmospheric Corrosion Resistance of Austenitic Stainless Steels" Effects of Residual Elements on Properties of Austenitic Stainless Steels, American Society for Testing and Materials, p. 3 (1967)

[14] N.D. Tomashov, G.P. Chernova, and O.N. Marcove. Corrosion, Vol 20, p. 166 (1964)

[15] S. Bernhardsson, "The Corrosion Resistance of Duplex Stainless Steels", Duplex Stainless Steels '91, Vol 1, p. 187 (1991)

[16] S. Bernhardsson, "The Corrosion Resistance of Duplex Stainless Steels", Duplex Stainless Steels '91, Vol 1, p. 196 (1991)

[17] Z. Szklarska-Smialowska. Pitting Corrosion of Metals, 1st ed. National Association of Corrosion Engineers, p. 236 (1986)

[18] R.J. Bingham and E.W. Tozer. Corrosion, Vol. 29, p. 33 (1973)

[19] G.R. Youngquist. Chemical Engineering Education, p. 20 (Winter, 1979)

[20] E.C. Potter. Electrochemistry Principles and Applications, 1st ed. Cleaver-Hume Press Ltd., p. 57 (1956)

[21] CMS100 Corrosion Measurement System Operator's Manual, Revision 2.00. Gamry Instruments Inc., p 1-7 (1992)

Appendix A

The following pages contain material test reports on the alloys used in the laboratory experiments. The reports give the elemental compositions of the specific samples in weight percent. The physical properties and conditioning are also included for reference. The reports contain data on samples used in this study as well as another related investigation. The samples used for this thesis are indicated with an asterix, *.

METAL SAMPLES CO.

P.O. BOX 8
RT 1 BOX 152
MUNFORD, AL 36268
(205) 358-4202
FAX (205) 358-4515

MATERIAL TEST REPORT

DATE: 06/14/94

CUSTOMER: UNIVERSITY OF SASKATCHEWAN

CUST. ORDER: K189800

M.S. ORDER: 943051

DEAR CUSTOMER:
WE CERTIFY THAT THIS MATERIAL TEST REPORT IS CORRECT TO THE BEST OF OUR KNOWLEDGE AND THAT THE MATERIAL SUPPLIED MEETS THE REQUIRED SPECIFICATIONS.
THANK YOU.

QUALITY CONTROL DEPARTMENT

CHEMICAL PROPERTIES

	ALLOY	HEAT	AL	C	CR	CU	FE	MN	MO	NI	P	S	SI	TI	OTHERS
	430	G017	0.014	0.046	16.28	0.12	BAL	0.41	0.02	0.14	0.023	0.005	0.42		V-0.05; SN-0.02; CO-0.0
															3; CB-0.01; N-0.037
*	430	D723	<0.005	0.036	16.60	0.10	BAL	0.50	0.040	0.31	0.028	0.013	0.53		
*	304LN	D450		0.021	19.80	0.18	BAL	1.80	0.40	8.80	0.034	0.008	0.45		CO-0.12; N-0.124
*	CN7M	G520		0.056	20.02	3.32	43.591	1.10	2.18	28.79	0.026	0.007	0.91		
	316L	H844		0.013	16.12	0.32		1.60	2.01	10.05	0.033	0.025	0.32		CO-.16; N-.05
*	316L	E778		0.020	17.47	0.360	BAL	1.61	2.290	11.70	0.023	0.025	0.590		CO-0.11; N2-0.085
	A53GRB	E620		0.17			BAL	0.65			0.019	0.007	0.02		
	347	0986		0.063	17.19	0.18	BAL	1.49	0.29	9.30	0.022	0.004	0.51		CO-0.03; TA-0.006; C+T-
															0.80
*	347	H276		0.052	17.14	0.25	BAL	1.78	0.23	9.96	0.021	0.002	0.47		CB+TA-.80

PHYSICAL PROPERTIES

	ALLOY	HEAT	TENSILE - KSI	YIELD - KSI	ELONG - %	R / A - %	HARDNESS	COND.	UNS	MILL
	430	G017	85.7	75.5	18.0	73.0	BHN 160		S43000	LTV STEEL
*	430	D723						ANN	S43000	ALTECH
*	304LN	D450	86.5	41.4	60.0	71.0	BHN 174	ANN	S30453	JESSOP
*	CN7M	G520							J95150	TEXAS STAINLESS
	316L	H844	99.7	81.9	35 (2")	65.4	RB 95		S31603	INDUSTRIAL ALLOYS
*	316L	E778	95.0	73.0	42.0	73.0	BHN 197	ANN	S31603	ALTECH
	A53GRB	E620	70.1	46.9	42.0				K03005	LABARGE
	347	0986	106.0	79.0	43.0	70.0	BHN 235		S34700	ALTECH
*	347	H276	104.8	79.7	42 (2")	68.6	BHN 240		S34700	SOUTHERN TOOL STEEL

* Used in Laboratory Expts.

METAL SAMPLES CO.

P.O. BOX 8
RT 1 BOX 152
MUNFORD, AL 36268
(205) 358-4202
FAX (205) 358-4515

MATERIAL TEST REPORT

DATE: 06/14/94

CUSTOMER: UNIVERSITY OF SASKATCHEWAN

CUST. ORDER: K189800

M.S. ORDER: 943051

DEAR CUSTOMER:
WE CERTIFY THAT THIS MATERIAL TEST REPORT IS CORRECT TO THE BEST OF OUR KNOWLEDGE AND THAT THE MATERIAL SUPPLIED MEETS THE REQUIRED SPECIFICATIONS.
THANK YOU.

Gary Bear
QUALITY CONTROL DEPARTMENT

CHEMICAL PROPERTIES

	ALLOY	HEAT	AL	C	CR	CU	FE	MN	MO	NI	P	S	SI	TI	OTHERS
	17-4PH	D737		0.034	15.57	3.860	BAL	0.45	0.130	4.28	0.020	0.023	0.340		N2-0.016; CB+TA-0.28; B<0.01
*	17-4PH	D706		.05	15.38	3.20	BAL	.43	.43	4.31	.027	.012	.60		CB-.32; TA-.01
*	304L	G424		0.02	18.18	0.30	BAL	1.83	0.29	9.74	0.023	0.026	0.30	<0.01	CB-<0.01; CO-0.09; N-0.082; TA-<0.01; V-0.08
*	304L	D768		0.012	18.22	0.250	BAL	1.54	0.240	8.77	0.029	0.022	0.560	<0.01	N2-0.063; CO-0.12; CB-0.01; TA-<0.01
	446	C007		0.11	24.35		BAL	0.51			0.024	0.006	0.53		N-0.17
*	446	0963		0.092	25.97		BAL	1.29			0.017	0.022	0.66		N2-0.18
	904L	F752		0.014	20.90	1.50	BAL	1.67	4.44	24.45	0.025	0.009	0.49		N-.035; CO-.17
*	904L	E390		0.016	20.27	1.36	BAL	1.82	4.32	24.04	0.024	0.003	0.15		
	2205	F754		.016	21.97	.13	BAL	1.49	2.99	5.85	.024	.001	.59		CO-.06; N-.16

PHYSICAL PROPERTIES

	ALLOY	HEAT	TENSILE - KSI	YIELD - KSI	ELONG - %	R / A - %	HARDNESS	COND.	UNS	MILL
	17-4PH	D737					BHN 341	ANN	S17400	ALTECH
*	17-4PH	D706					Rc 35		S17400	FRY
*	304L	G424	104.5	72	39 (2")	70	BHN 217	SOLANN	S30403	AL TECH
*	304L	D768	92.0	60.0	51	68	BHN 179	ANN	S30403	ALTECH
	446	C007	88.95	75.18	24.5	59.3	Rb 91		S44600	CRUCIBLE
*	446	0963	78.0	54.9	32.1	64.2	Rb 80	HTRDAN	S44600	ROLLED ALLOYS
	904L	F752	83.2	37.4	53.7	65.8	BHN 143		N08904	JESSOP
*	904L	E390							N08904	THYSSEN
	2205	F754	109.8	71.2	41.8	71.0	BHN 217		S31803	JESSOP STEEL

* Used in Laboratory Expts

METAL SAMPLES CO.

P.O. BOX 8
RT 1 BOX 152
MUNFORD, AL 36268
(205) 358-4202
FAX (205) 358-4515

MATERIAL TEST REPORT

DATE: 06/14/94

CUSTOMER: UNIVERSITY OF SASKATCHEWAN

CUST. ORDER: K189800

M.S. ORDER: 943051

DEAR CUSTOMER:
WE CERTIFY THAT THIS MATERIAL TEST REPORT IS CORRECT TO THE BEST OF OUR KNOWLEDGE AND THAT THE MATERIAL SUPPLIED MEETS THE REQUIRED SPECIFICATIONS.
THANK YOU.

QUALITY CONTROL DEPARTMENT

CHEMICAL PROPERTIES

	ALLOY	HEAT	AL	C	CR	CU	FE	MN	MO	NI	P	S	SI	TI	OTHERS
*	2205	G614		0.016	22.20		BAL	1.52	3.00	5.60	0.025	0.002	0.34		N-0.15
	C276	J196		0.003	15.47		5.70	0.48	15.70	BAL	<0.005	0.002	0.03		CO-1.32;V-.15;W-3.31
	C276	D968		<0.002	15.48		5.88	0.46	15.60	BAL	0.008	0.002	0.04		CO-0.43; V-0.12; W-3.

PHYSICAL PROPERTIES

	ALLOY	HEAT	TENSILE - KSI	YIELD - KSI	ELONG - %	R / A - %	HARDNESS	COND.	UNS	MILL
*	2205	G614	111.8 KSI	71.7 KSI	44.1% (2")	83.1%	RB 98	SOL AN	S31803	AVESTA
	C276	J196	111.0	46.0	67.0	ASTMB57491		ANLD	N10276	HAYNES INT'L
	C276	D968	109.0	59.0	69.0				N10276	CABOT

* Used in Laboratory Expts.

Metal Samples
P.O. BOX 8 • 152 METAL SAMPLES RD.
MUNFORD, AL 36268
(205) 358-4202 • FAX (205) 358-4515

MATERIAL TEST REPORT

DATE: 12/02/94

CUSTOMER: UNIVERSITY OF SASKATCHEWAN

CUST. ORDER: L198367

M.S. ORDER: 946846

DEAR CUSTOMER:
WE CERTIFY THAT THIS MATERIAL TEST REPORT IS CORRECT TO THE BEST OF OUR KNOWLEDGE AND THAT THE MATERIAL SUPPLIED MEETS THE REQUIRED SPECIFICATIONS.
THANK YOU.

QUALITY CONTROL DEPARTMENT

CHEMICAL PROPERTIES

	ALLOY	LOT	AL	C	CR	CU	FE	MN	MO	NI	P	S	SI	TI	OTHERS
*	254SMO	D056		.009	20.10	.74	BAL	.44	6.15	18.0	.028	.001	.31		N-.200
*	CD4MCU	J315		0.022	25.52	2.89	62.96	0.78	1.87	5.04	0.039	0.019	0.86		

PHYSICAL PROPERTIES

	ALLOY	LOT	TENSILE - KSI	YIELD - KSI	ELONG - %	R/A - %	HARDNESS	COND.	UNS	MILL
*	254SMO	D056							S31254	AVESTA
*	CD4MCU	J315	103.766	73.65	60.6			ANNLD	J93370	TEXAS STAINLESS

* Used in laboratory Expts.

Metal Samples
P.O. BOX 8 • 152 METAL SAMPLES RD.
MUNFORD, AL 36268
(205) 358-4202 • FAX (205) 358-4515

MATERIAL TEST REPORT

DATE: 02/02/95
CUSTOMER: UNIVERSITY OF SASKATCHEWAN
CUST. ORDER: K200099
M.S. ORDER: 950503

DEAR CUSTOMER:
WE CERTIFY THAT THIS MATERIAL TEST REPORT IS CORRECT TO THE BEST OF OUR KNOWLEDGE AND THAT THE MATERIAL SUPPLIED MEETS THE REQUIRED SPECIFICATIONS.
THANK YOU.

QUALITY CONTROL DEPARTMENT

CHEMICAL PROPERTIES

ALLOY	HEAT	AL	C	CR	CU	FE	MN	MO	NI	P	S	SI	TI	OTHERS
AF2304	J496		0.030 MAX	22.0/23 .5	0.10/0. 60		2.0 MAX	0.10/0. 6	4.0/5.0	0.035 MAX	0.010 MAX	0.7 MA X		N-0.08/0.15
16LN	D447		0.020	16.52	0.27	BAL	1.77	2.08	10.15	0.030	0.015	0.56		CO-0.12; N-0.119

PHYSICAL PROPERTIES

ALLOY	HEAT	TENSILE KSI	YIELD KSI	ELONG %	R/A %	HARDNESS	COND.	UNS	MILL
AF2304	J496	99.5	68.5					S32304	AVESTA
316LN	[illegible]	[illegible]	[illegible]	52	67	Rb 78/79	ANN	S31653	IRSID

* Used in Laboratory Expts.

PAGE 1 of _____